Available on CMS information server

CMS NOTE 2006/136

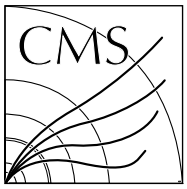

The Compact Muon Solenoid Experiment

CMS Note

Mailing address: CMS CERN, CH-1211 GENEVA 23, Switzerland

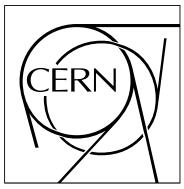

July 18, 2006

Search for the Standard Model Higgs Boson in the Two-Electron and Two-Muon Final State with CMS

D. Futyan, D. Fortin

University of California, Riverside, USA

D. Giordano

Università di Bari and INFN, Italy

Abstract

The decay of the Standard Model Higgs boson to $ZZ^{(\star)}$, with both Zs decaying to leptons is one of the most important potential discovery channels for the Higgs boson at the LHC. The four lepton state with the highest branching ratio is the two-electron two-muon final state. This note presents the discovery potential of the Higgs boson using this channel at CMS for Higgs boson masses between 115 and 600 GeV. It is found that a Higgs boson with mass in the range 130 GeV$\leq \mathrm{m_H} \leq$ 500 GeV, excluding a narrow region close to $\mathrm{m_H}$ = 170 GeV is expected to be observable at CMS with a significance exceeding 5σ with 30 fb^{-1} of integrated luminosity.

1 Introduction

The mass of the Higgs boson ($\mathrm{m_H}$) is the only unknown parameter in the Higgs sector of the Standard Model (SM). Direct searches at LEP yield lower bounds of $\mathrm{m_H} > 114.4$ GeV at the 95% confidence level [2]. In addition, fits to electroweak precision measurements from LEP, SLC and Tevatron lead indirectly to an upper bound of $\mathrm{m_H} < 207$ GeV [1] at the 95% confidence level.

The dominant production mechanisms for the SM Higgs boson at the LHC, over the entire mass range, are gluon fusion gg→H and vector boson fusion $\mathrm{q\overline{q}} \rightarrow \mathrm{q\overline{q}H}$ as illustrated in Figure 1. The dominant branching fractions for the decay of the Higgs boson are shown in Figure 2. It can be seen that for $\mathrm{m_H} > 130$GeV, the decay is almost entirely through the $\mathrm{H} \rightarrow \mathrm{W^+W^-}$and $\mathrm{H} \rightarrow \mathrm{ZZ^{(\star)}}$ channels.

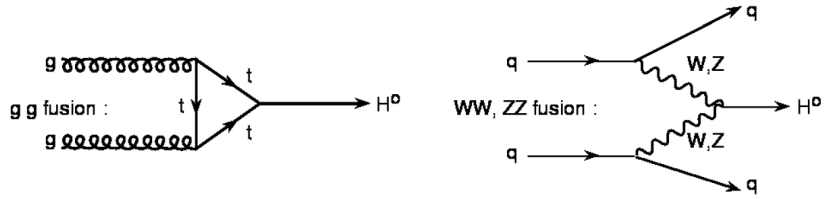

Figure 1: Main production mechanisms of the Higgs boson at the LHC.

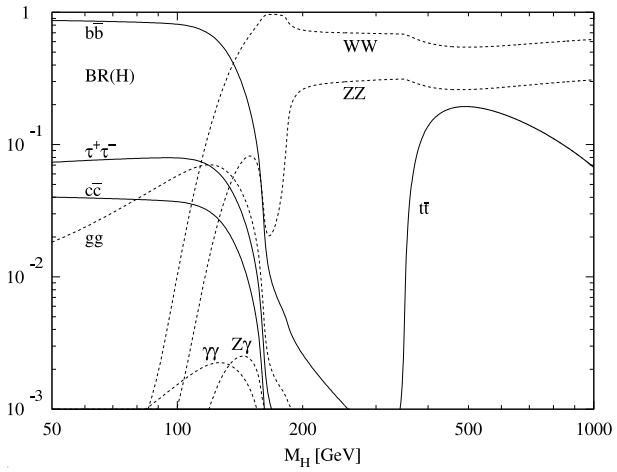

Figure 2: Branching fractions for the SM Higgs boson as a function of $\mathrm{m_H}$ calculated using the HDECAY program [3]

The $\mathrm{H} \rightarrow \mathrm{ZZ^{(\star)}} \rightarrow 4\ell$ channel yields a very clean signature with relatively small backgrounds and is therefore an important potential discovery channel for the Higgs boson for a large range of masses. The channel is also important for the measurement of the mass and width of the Higgs boson. For $\mathrm{m_H}$ between 130 GeV and 500 GeV, this channel has the highest sensitivity for the discovery of the Higgs boson at CMS, except in the range 150 GeV$< \mathrm{m_H} <$190 GeV, where the $\mathrm{H} \rightarrow \mathrm{W^+W^-} \rightarrow 2\ell 2\nu$ channel is more sensitive, due to the branching ratio $\mathrm{H} \rightarrow \mathrm{W^+W^-}$ being enhanced while the $\mathrm{H} \rightarrow \mathrm{ZZ^{(\star)}}$ branching ratio is suppressed (see Figure 2). For $\mathrm{m_H}$ <130 GeV, the $\mathrm{H} \rightarrow \gamma\gamma$ channel should yield the highest sensitivity, though the backgrounds are much larger than for $\mathrm{H} \rightarrow \mathrm{ZZ^{(\star)}} \rightarrow 4\ell$.

This note presents the discovery potential of the Higgs boson at CMS for the $2e2\mu$ final state in $H \rightarrow ZZ^{(\star)} \rightarrow 4\ell$. This channel is important since although electron detection efficiencies are lower than for muons, the branching ratio is twice that in 4μ and 4e final states.

2 Event Generation

All simulated event samples used in the analysis were generated using the PYTHIA 6.152 [4] event generator, except for the $Zb\bar{b}$ ($e^+e^-b\bar{b}$ and $\mu^+\mu^-b\bar{b}$) background samples which were generated with CompHEP 4.2 [5].

The effect of final state radiation (internal bremsstrahlung) was simulated in all samples using the PHOTOS [6] software package.

The Z bosons in the signal and in the $ZZ^\star/\gamma^\star$background, and the W bosons in the $t\bar{t}$ background, were forced to decay to electrons, muons or taus, and in the case of decay to taus, the taus were forced to decay to electrons or muons. The forcing of taus to decay to electrons or muons has the consequence that events in which one or both Zs decay to taus are over-represented in the generated event samples because their suppression due to the $\tau \rightarrow e/\mu$ branching ratio is absent. This is taken into account in the analysis as described in Appendix A.

For all simulated samples, a preselection is applied at generator level with the following requirements:

1. Final state contains $e^+e^-\mu^+\mu^-$;
2. $p_T(e) > 5$ GeV and $|\eta(e)| < 2.7$ for both electrons;
3. $p_T(\mu) > 3$ GeV and $|\eta(\mu)| < 2.4$ for both muons.

At analysis level, a tighter requirement is applied to the pseudorapidity of the generated electrons to require that they lie within the fiducial region of the electromagnetic calorimeter (ECAL), defined as $|\eta| < 2.5$. Preselection efficiencies in this note refer to these cuts.

2.1 Higgs Boson Signal

The $H \rightarrow ZZ^{(\star)} \rightarrow 2e2\mu$ signal samples were generated with PYTHIA, including Leading Order gluon and vector boson fusion processes. Samples of 10000 events each were generated for 18 values of m_H ranging from 115 GeV to 200 GeV in 10 GeV steps, and from 200 GeV to 600 GeV in 50 GeV steps.

The SM Higgs boson production cross-section calculated at Next to Leading Order using the HIGLU program [9], including production through gluon fusion and vector boson fusion, is shown as a function of the Higgs boson mass in Figure 3(a). The branching ratio of the Higgs boson to a final state containing four leptons (both e or μ), calculated using the HDECAY program [3] is shown as a function of the Higgs boson mass in Figure 3(b). This branching ratio includes decays of the $Z^{(\star)}$ to $\tau^+\tau^-$ with both taus decaying to e or μ.

The cross-section times branching ratio and the cross-section times branching ratio times preselection efficiency, are shown as a function of the Higgs boson mass in Figure 4.

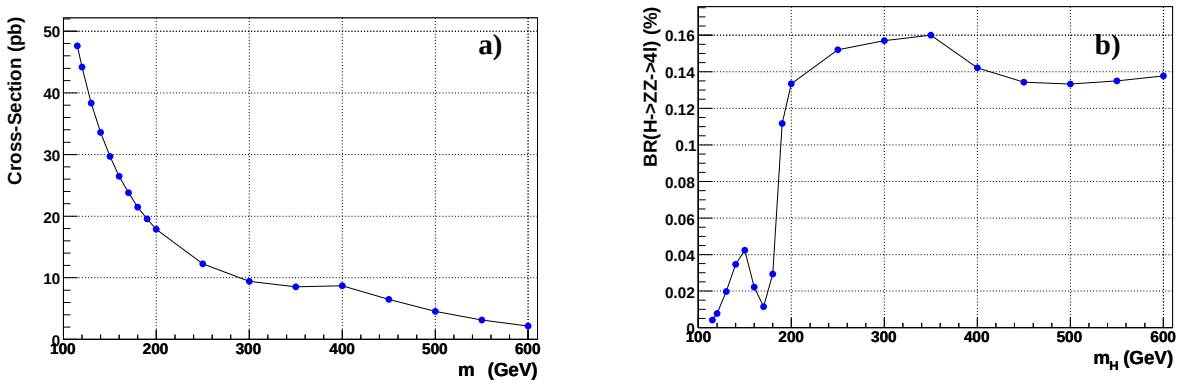

Figure 3: (a) Next to Leading Order production cross-section for the Standard Model Higgs boson, and (b) Branching ratio of the Standard Model Higgs boson to a final state containing four leptons (both e or μ).

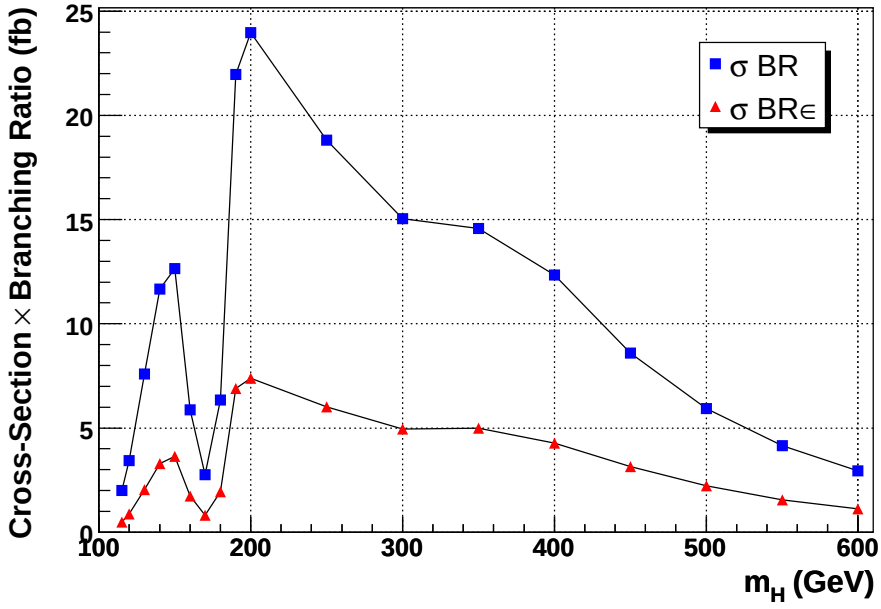

Figure 4: Cross-section times branching ratio, and cross-section times branching ratio times preselection efficiency for $H \rightarrow ZZ^{(\star)} \rightarrow 2e2\mu$.

2.2 Background Processes

Three background processes which yield the same signature of two electrons and two muons in the final state, with significant cross-section times branching ratio, are considered:

1. $q\overline{q}/gg \rightarrow t\overline{t} \rightarrow W^+W^-b\overline{b} \rightarrow e^+e^-\mu^+\mu^-X$: 312000 events generated with PYTHIA. No restrictions on b decays were applied.
2. $q\overline{q}/gg \rightarrow Zb\overline{b} \rightarrow e^+e^-\mu^+\mu^-X$: Generated with CompHEP, with $|\eta_b| < 2.5$. No restrictions on b decays were applied. Events were generated separately for:
   (a) $q\overline{q}/gg \rightarrow e^+e^-b\overline{b} \rightarrow e^+e^-\mu^+\mu^-X$ (188000 events)
   (b) $q\overline{q}/gg \rightarrow \mu^+\mu^-b\overline{b} \rightarrow e^+e^-\mu^+\mu^-X$ (63000 events)
3. $q\overline{q} \rightarrow ZZ^\star/\gamma^\star \rightarrow e^+e^-\mu^+\mu^-$: 10000 events generated with PYTHIA, with $m_{\gamma^\star} > 5$ GeV. t-channel $q\overline{q}$ fusion only (gg fusion and s-channel $q\overline{q}$ fusion not available in PYTHIA).

The potential background contribution from $Zc\overline{c} \rightarrow e^+e^-\mu^+\mu^-X$ was also investigated using fully simulated events and was shown to be negligible.

The leading order cross-section, K-factor, next to leading order cross-section and the cross-section times branching ratio times preselection efficiency are shown for each background process in Table 1.

Process	$\sigma_{\rm LO}$ (pb)	K-factor	$\sigma_{\rm NLO}$ (pb)	$\sigma_{\rm NLO}$.BR.ϵ (fb)
$t\overline{t} \rightarrow W^+W^-b\overline{b} \rightarrow e^+e^-\mu^+\mu^-X$	-	-	840	743
$e^+e^-b\overline{b} \rightarrow e^+e^-\mu^+\mu^-X$	115	2.4	276	262
$\mu^+\mu^-b\overline{b} \rightarrow e^+e^-\mu^+\mu^-X$	116	2.4	279	128
$ZZ^\star/\gamma^\star \rightarrow e^+e^-\mu^+\mu^-$	18.7	$K_{NLO}(m_{4\ell}) + 0.2$	28.9	37.0

Table 1: LO cross-section, K-factor, NLO cross-section and the cross-section times branching ratio times preselection efficiency for the three background process.

For the $t\overline{t}$ background, the NLO production cross-section is taken from [10]. For the $e^+e^-b\overline{b}$ and $\mu^+\mu^-b\overline{b}$ processes the LO cross-sections are those calculated by CompHEP, and the K-factor has been calculated [11] using MCFM. In the remainder of this note, the $e^+e^-b\overline{b}$ and $\mu^+\mu^-b\overline{b}$ processes are considered together and are referred to as $Zb\overline{b}$.

For the $ZZ^\star/\gamma^\star$ background, in order to account for contributions from all NLO diagrams and from the NNLO gluon fusion ($gg \rightarrow ZZ^\star/\gamma^\star$), all events are re-weighted at analysis level with an $m_{4\ell}$ dependent K-factor $K(m_{4\ell}) = K_{NLO}(m_{4\ell}) + 0.2$. The NLO K-factor $K_{NLO}(m_{4\ell})$ was calculated [11][12] with MCFM and is shown in Figure 5. The NNLO gluon fusion process has been shown using the TOPREX generator to contribute approximately 20% with respect to leading order. The NLO cross section shown in Table 1 uses the average value of 1.35 for $K_{NLO}(m_{4\ell})$.

3 Detector Simulation and Event Reconstruction

The generated Monte Carlo events for each dataset were processed through a full simulation of the CMS detector using CMSIM (CMS Simulation) [7]. This was in turn followed by digitization and inclusion of simulated pileup at low luminosity ($2 \times 10^{33}\mathrm{cm}^{-2}\mathrm{s}^{-1}$) and finally

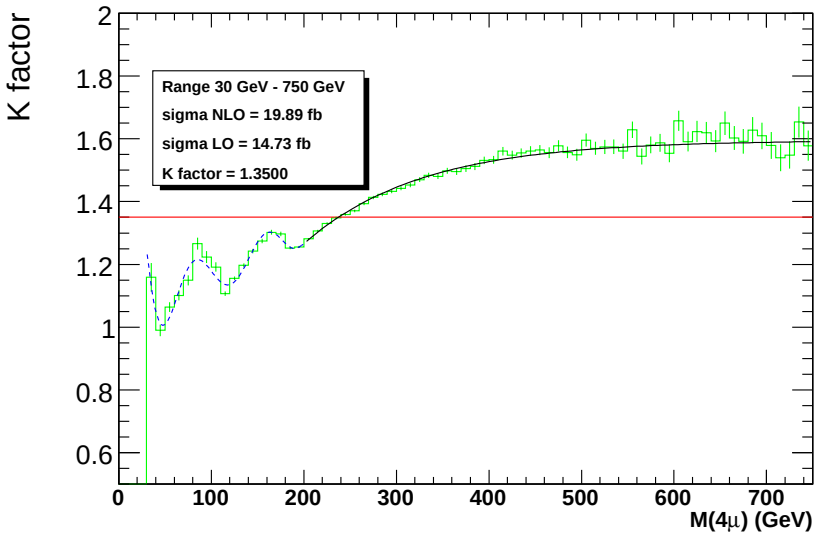

Figure 5: The $m_{4\ell}$ dependent K-factor $K_{NLO}(m_{4\ell})$ for the ZZ$^\star/\gamma^\star$ process, evaluated [11][12] using MCFM.

reconstruction of physics objects using ORCA (Object-oriented Reconstruction for CMS Analysis) [8].

4 Online Selection

A detailed investigation of the choice of trigger events for the analysis was performed. It was found that taking the logical OR of the di-muon and di-electron triggers yields high signal efficiency while suppressing the rate for the largest background, $\mathrm{t\bar{t}}$, by almost a factor of three. This is the natural choice of trigger from a physics viewpoint since most events will contain at least one real Z, so to require a di-electron or di-muon trigger is effectively to trigger on the Z. It was found that the use of single electron and single muon triggers does not benefit the final significance obtained from the analysis.

The efficiencies of the Level-1 and High Level Triggers are shown for the signal as a function of $\mathrm{m_H}$ in Figure 6. The HLT efficiency is shown for events which have passed the Level-1 trigger. The corresponding trigger efficiencies for background processes are shown in Table 2. The trigger tables used are those described in Volume 1 of the CMS Physics TDR [16].

	$\mathrm{t\bar{t}}$	$\mathrm{Zb\bar{b}}$	ZZ$^\star/\gamma^\star$
Level-1 Trigger efficiency (%)	95.1±0.1	92.3±0.1	97.9±0.2
HLT efficiency (%)	39.9±0.1	65.8±0.1	89.6±0.4

Table 2: Efficiency of the Level-1 and High Level Triggers for each of the three background processes. Statistical errors are shown.

5 Offline Reconstruction

Offline reconstruction of electrons and muons is performed using standard ORCA algorithms. The most recent developments in electron reconstruction described in [13] are applied here,

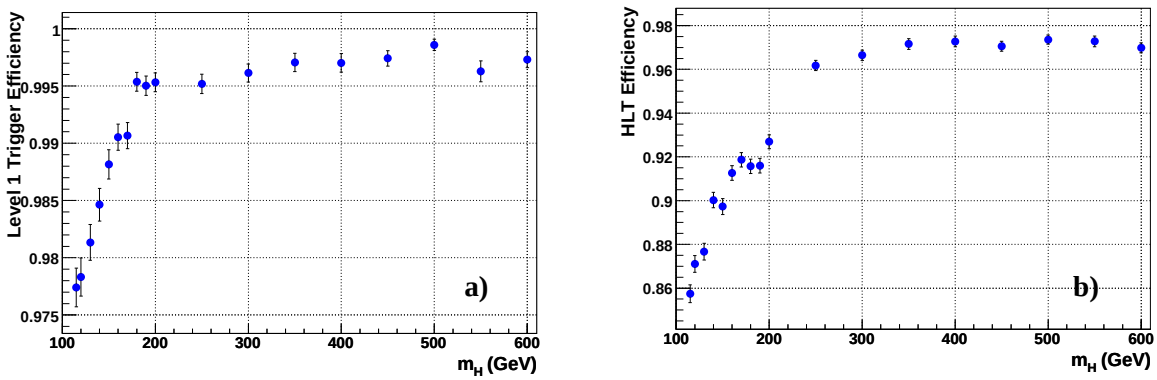

Figure 6: Efficiency of the Level-1 (a) and High Level Triggers (b) for the Higgs boson signal.

which allows electron tracks to be reconstructeds right out to the electromagnetic calorimeter (ECAL), optimal combination of information from the ECAL cluster and the track, and optimized cuts for ECAL and track seeding. The new cuts result in a substantial increase in reconstruction efficiency for low p_T electrons.

The first step in the offline event selection is to require that four leptons of type $\mathrm{e^+e^-\mu^+\mu^-}$ are reconstructed. The efficiency for reconstructing $\mathrm{e^+e^-\mu^+\mu^-}$ offline for events selected by the High Level Trigger is shown for the signal as a function of $\mathrm{m_H}$ in Figure 7. The efficiency for reconstructing $\mathrm{e^+e^-\mu^+\mu^-}$ offline for background processes are shown in Table 3.

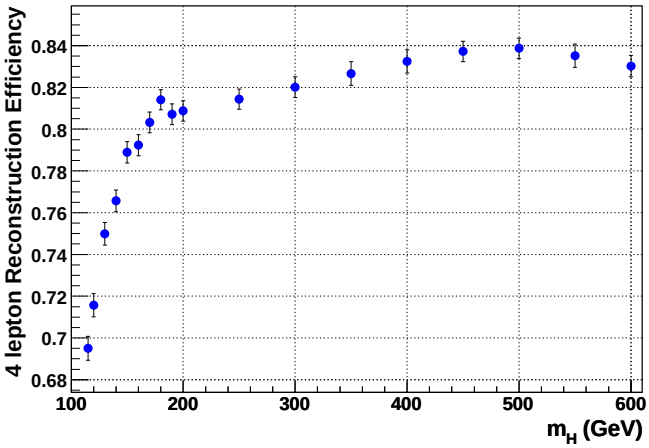

Figure 7: Efficiency for reconstructing $\mathrm{e^+e^-\mu^+\mu^-}$ offline for the Higgs boson signal.

	$\mathrm{t\bar{t}}$	$\mathrm{Zb\bar{b}}$	$\mathrm{ZZ^\star/\gamma^\star}$
$\mathrm{e^+e^-\mu^+\mu^-}$ reconstruction efficiency (%)	46.1±0.2	59.5±0.1	74.2±0.6

Table 3: Efficiency for reconstructing $\mathrm{e^+e^-\mu^+\mu^-}$ offline for each of the three background processes. Statistical errors are shown.

5.1 Electron Identification

The number of candidate reconstructed electrons is greater than two for a significant fraction of events due to fakes, arising for example, due to $\pi^+\pi^0$ overlap or π^0 conversions from the underlying event. A likelihood approach has been found to provide strong discrimination between real and fake candidates.

The likelihood combines information from the following variables:

1. Difference in pseudorapidity between the track and the ECAL super-cluster;
2. Ratio of ECAL energy to track momentum;
3. Ratio of HCAL energy to ECAL energy;
4. Ratio of 3×3 to 5×5 crystal energy sums in the ECAL cluster;
5. Shower spread in the longitudinal direction, given by the covariance matrix element for a 5×5 array of ECAL crystals: $\sigma_{\eta\eta} = \sum_{5\times5}[(\eta_i - \eta_{max})^2 E_i/E_{5\times5}]$, where η_i and E_i are the pseudorapidity and energy of the i^{th} crystal and η_{max} is the pseudorapidity of the largest energy crystal.

The likelihood of a candidate reconstructed electron being consistent with hypothesis ψ (real electron or fake electron), given set of values **x** for the discriminating variables is given by:

$$L(\mathbf{x};\psi) = \prod_{i=1}^{5} P_i(x_i;\psi)$$

where $P_i(x_i;\psi)$ is the probability density function for variable i having value x_i, given hypothesis ψ. The PDFs are constructed in the form of reference histograms. Those for real electrons were constructed using electrons matched to generator level electrons in Higgs boson signal events; those for fakes were constructed using jet background Monte Carlo samples covering a broad spectrum of jet p_T (p_T >25GeV). All reference histograms were constructed separately for barrel and endcaps.

The likelihood ratio used to discriminate between real and fake electrons is then given by:

$$LR = \frac{L(\mathbf{x};electron)}{L(\mathbf{x};electron) + L(\mathbf{x};fake)}$$

Reconstructed electrons are required to have $LR > 0.2$. For each event, the electron candidate with the highest likelihood ratio is selected for each charge. This was found to give significantly better performance than selecting the highest p_T electron candidates for each charge.

5.2 Vertex Fit

The primary vertex is reconstructed by performing a fit to the tracks of the four reconstructed leptons using the Kalman filter formalism [14]. The lepton tracks are then refitted using the reconstructed vertex position as an additional point, in order to obtain a more accurate measurement of the momentum at the primary vertex.

5.3 Reconstructed Z Boson Mass

For a Higgs boson mass of 130 GeV, Figure 8 shows the distributions of the reconstructed invariant masses of the e^+e^- and $\mu^+\mu^-$ pairs, together with the distribution of the ratio of the measured to the true invariant mass for each case. Figure 9 shows the reconstructed invariant mass of the $\mu^+\mu^-$ pair plotted against that of the e^+e^- pair, also for m_H = 130 GeV. It can be seen that one of the Z bosons is always on shell, as expected.

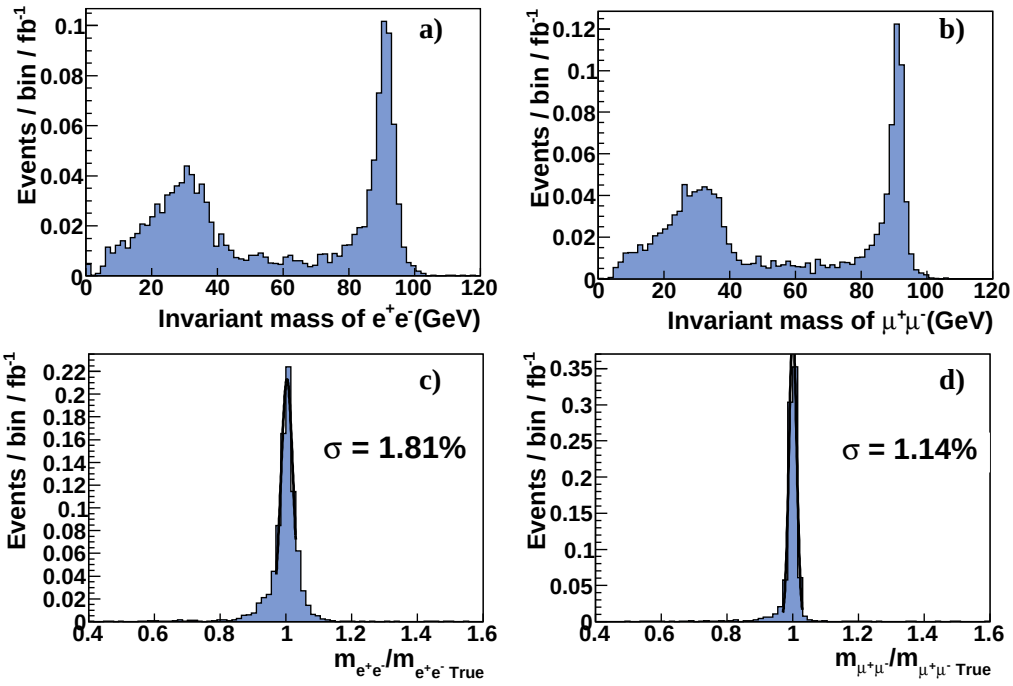

Figure 8: Reconstructed invariant masses of the e^+e^- (a) and $\mu^+\mu^-$ (b) pairs; ratio of measured to true invariant mass for the e^+e^- (c) and $\mu^+\mu^-$ (d) pairs, for m_H = 130 GeV.

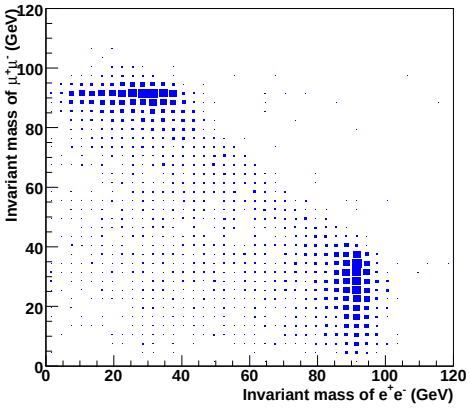

Figure 9: Reconstructed invariant mass of the $\mu^+\mu^-$ pair plotted against that of the e^+e^- pair, for m_H = 130 GeV.

5.4 Recovery of Internal Bremsstrahlung

Internal or inner bremsstrahlung refers to the final state QED radiation of a photon at the primary vertex from one of the final state leptons. At least one such photon is present in 40-45% of $H \rightarrow ZZ^{(\star)} \rightarrow 2e2\mu$ events (depending on m_H), and in 10% to 30% as m_H increases, there is at least one such photon with p_T >5 GeV. It was shown using generator level information that around two thirds of internal bremsstrahlung photons in $H \rightarrow ZZ^{(\star)} \rightarrow 2e2\mu$ events are emitted by an electron and one third emitted by a muon.

Internal bremsstrahlung photons can be distinguished from other photons from the underlying event from their strong tendency to be collinear with the direction of the parent lepton, as illustrated in Figure 10.

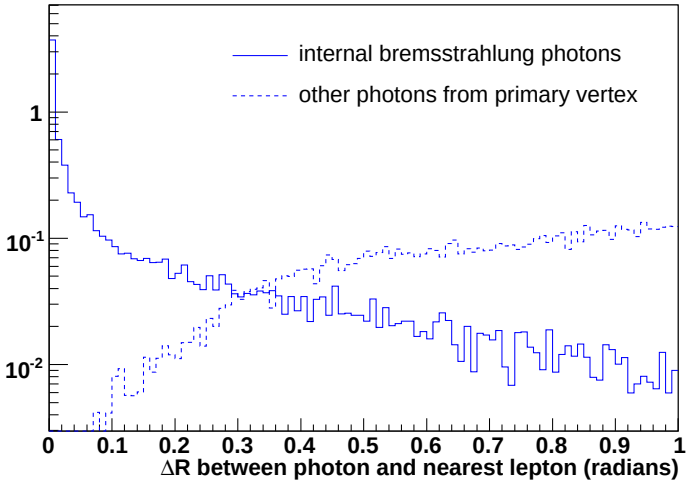

Figure 10: Angular separation, $\Delta R = \sqrt{\Delta\eta^2 + \Delta\phi^2}$, between generated internal bremsstrahlung photons with $p_T > 5$ GeV and their parent lepton (solid line), and between other photons from the primary vertex with $p_T > 5$ GeV and their nearest lepton (dashed line).

For each event, if one or more reconstructed photons are found within a cone of size $\Delta R = \sqrt{\Delta\eta^2 + \Delta\phi^2} < 0.3$ radians around any of the four reconstructed leptons, then the reconstructed photon with the smallest ΔR is considered to be a reconstructed internal bremsstrahlung photon. The four-momentum of this photon is added to that of the corresponding reconstructed Z boson prior to the Z mass window cuts described in Section 6.3.

Recovery of internal bremsstrahlung photons is found to increase the efficiency of the Z mass window cuts by around 1 to 2%, depending on m_H.

6 Offline Event Selection

The two largest backgrounds after the HLT, $t\bar{t}$ and $Zb\bar{b}$, are reducible, since unlike the Higgs boson signal, two of the leptons are associated with b-jets and therefore they are not isolated, and they have large impact parameter. These two features can be used to powerfully reject these processes. The ZZ background is in contrast irreducible by such means.

6.1 Vertex and Impact Parameter

An in depth study of how best to use information concerning compatibility of the lepton tracks, prior to the the four-lepton vertex fit, with originating from the primary event vertex has been performed. A number of possible discriminating quantities were investigated. The following three variables were chosen because they were found to be largely uncorrelated and have high background rejection for 95% signal efficiency:

1. Transverse distance from the vertex fitted to the $\mu^+\mu^-$ tracks to the nominal beam line (x=0,y=0): required to be less than 0.011 cm.

2. Three dimensional distance between the vertex fitted to the $\mu^+\mu^-$ tracks and the vertex fitted to the e^+e^- tracks: required to be less than 0.06 cm.

3. Transverse impact parameter significance of the lepton with the highest transverse impact parameter significance: required to be less than 7.

The distributions of the above three variables are shown for an example signal and for the $\mathrm{t\bar{t}}$ and $\mathrm{Zb\bar{b}}$ backgrounds in Figure 11.

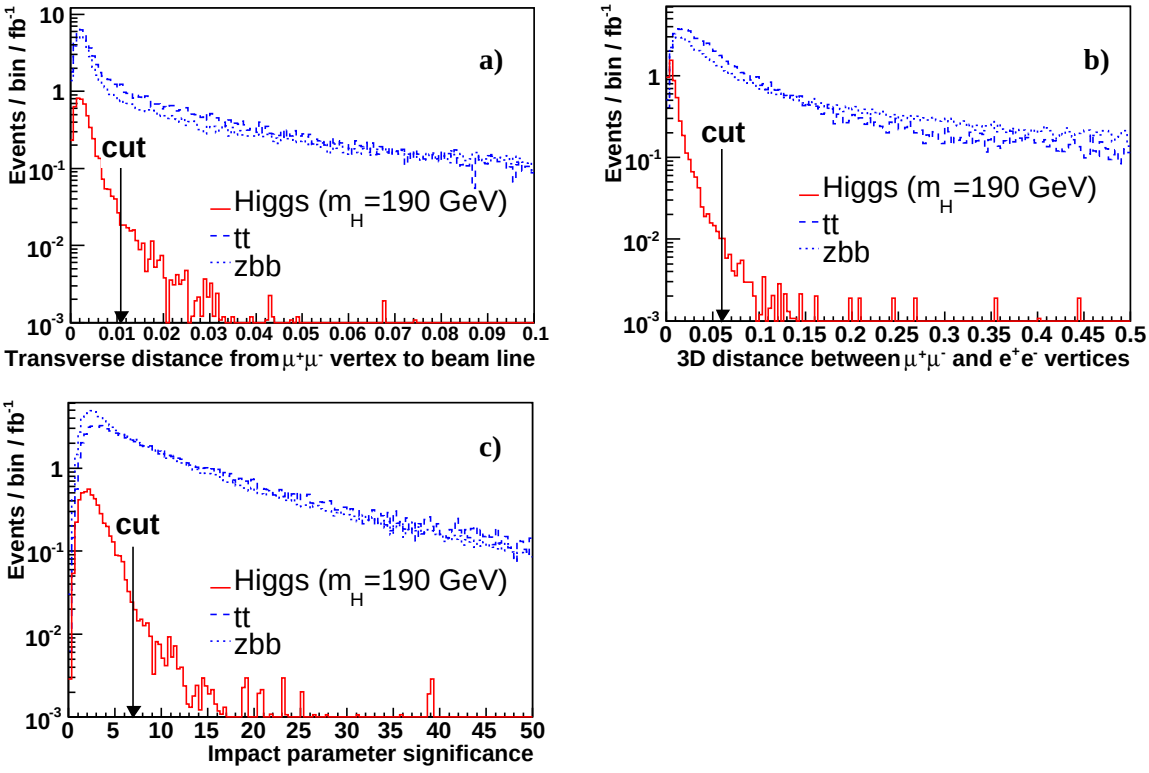

Figure 11: (a) Transverse distance from the vertex fitted to the $\mu^+\mu^-$ tracks to the nominal beam line. (b) Three dimensional χ^2 compatibility of the vertex fitted to the $\mu^+\mu^-$ tracks with the vertex fitted to the e^+e^- tracks. (c) Transverse impact parameter significance of the lepton with the highest transverse impact parameter significance.

Table 4 shows the combined efficiency of these cuts for the signal and for the $\mathrm{t\bar{t}}$ and $\mathrm{Zb\bar{b}}$ backgrounds. The signal selection efficiency is largely independent of $\mathrm{m_H}$: it ranges from 89% to 91% for the chosen set of cuts.

	Efficiency(%)
Signal	89-91
$\mathrm{t\bar{t}}$	14.5±0.2
$\mathrm{Zb\bar{b}}$	13.0±0.1

Table 4: Combined efficiency of the cuts on the three discriminating quantities for signal and for the $\mathrm{t\bar{t}}$ and $\mathrm{Zb\bar{b}}$ background processes. Statistical errors are shown for the background processes.

6.2 Isolation

The analysis currently considers isolation in the Tracker only. A cut is applied on the sum of the p_T of reconstructed tracks with $p_T > 0.9$ GeV and at least five reconstructed hits, which additionally satisfy the following requirements:

1. The track lies within the region defined by the sum of cones of size $\Delta\mathrm{R} < 0.25$ around each of the four leptons. Defining the isolation region as the sum of the cones around each lepton prevents double counting of tracks where cones overlap.
2. The track lies outside veto cones of size $\Delta\mathrm{R} > 0.015$ around each lepton.
3. The track is consistent with originating from the reconstructed primary vertex (see Section 5.2) to within $\Delta z < 0.2$cm, where Δz is the difference between the z position of the point of closest approach of the track to the reconstructed vertex, and the z position of the reconstructed vertex.

The Σp_T distribution of tracks selected as described above, is shown for an example signal ($\mathrm{m_H}$=190 GeV) and for the $\mathrm{t\bar{t}}$ and $\mathrm{Zb\bar{b}}$ backgrounds in Figure 12.

6.3 Kinematic Cuts

Cuts are applied on the following kinematic quantities:

1. Lepton p_T cuts:
   (a) $p_T^1 > thr1$
   (b) $p_T^2 > thr2$
   (c) $p_T^3 > thr3$
   (d) $p_T^4 > thr4$

   where p_T^1 to p_T^4 are the transverse momenta of the four reconstructed leptons in order of decreasing p_T. Figure 13 shows the lepton p_T distributions before offline selections, for four example signal masses, and for the three backgrounds.

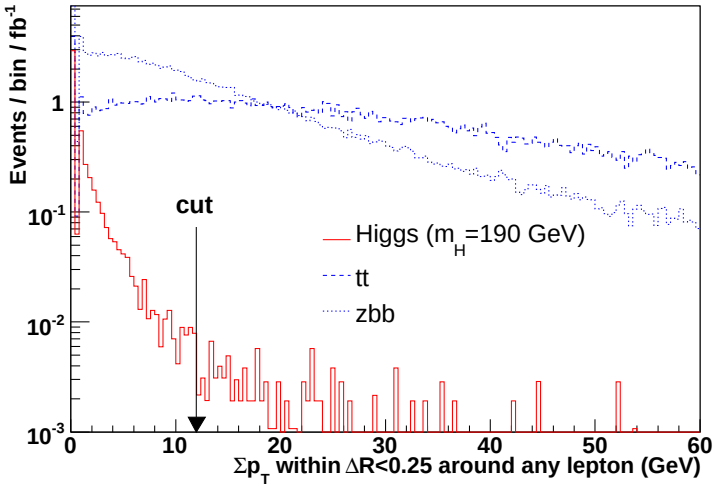

Figure 12: Sum of the p_T of reconstructed tracks with p_T >0.9 GeV and at least five hits, within the region defined by the sum of cones of size ΔR<0.25 around each of the four leptons, excluding a veto cone of size ΔR>0.015 around each lepton, and consistent with originating from the reconstructed primary vertex to within Δz <0.1cm, for $\mathrm{m_H}$=190 GeV, for $\mathrm{t\bar{t}}$ and $\mathrm{Zb\bar{b}}$.

2. Lepton pair invariant mass cuts. In the following, m_Z^1 and m_Z^2 are the invariant masses of the e^+e^- and $\mu^+\mu^-$ pairs, where m_Z^1 is defined to be greater than m_Z^2:

   (a) $m_Z^1 < thr5$

   (b) $m_Z^2 > thr6$

   Neither a lower cut on m_Z^1 nor an upper cut on m_Z^2 is applied, since it has been directly shown that such cuts do not give any additional background rejection when used in combination with the other kinematic cuts. Figure 14 shows the distributions of m_Z^1 and m_Z^2 before offline selections, for four example signal masses, and for the three backgrounds.

3. Four lepton invariant mass cuts:

   (a) $thr7 < \mathrm{m_H} < \mathrm{thr8}$

   where $\mathrm{m_H}$ is the invariant mass of the four reconstructed leptons.

The eight thresholds listed above plus the threshold on Σp_T for tracker isolation defined in Section 6.2 are optimized simultaneously using MINUIT [15], such that the log-likelihood ratio

$$S_L = \sqrt{2 \ln Q}, \qquad \text{where} \qquad Q = \left(1 + \frac{N_S}{N_B}\right)^{N_S+N_B} e^{-N_S} \tag{1}$$

is maximized. The optimization is performed separately for each Higgs boson mass.

The optimized values for all kinematics cuts are shown as a function of $\mathrm{m_H}$ in Figures 15 and 16.

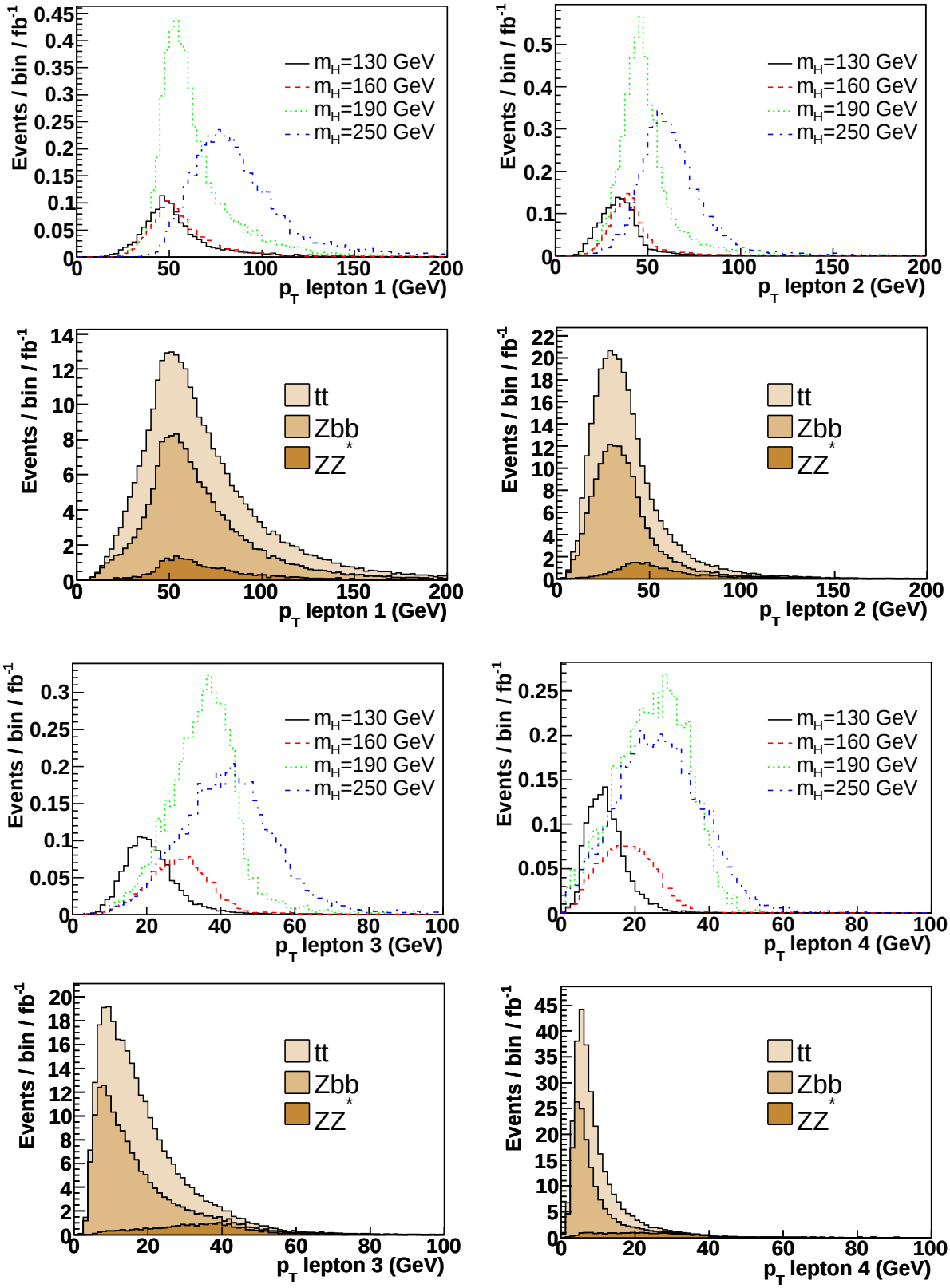

Figure 13: p_T distributions for the four reconstructed leptons, sorted in order of decreasing p_T, for m_H= 130, 160, 190 and 250 GeV, and for the three backgrounds.

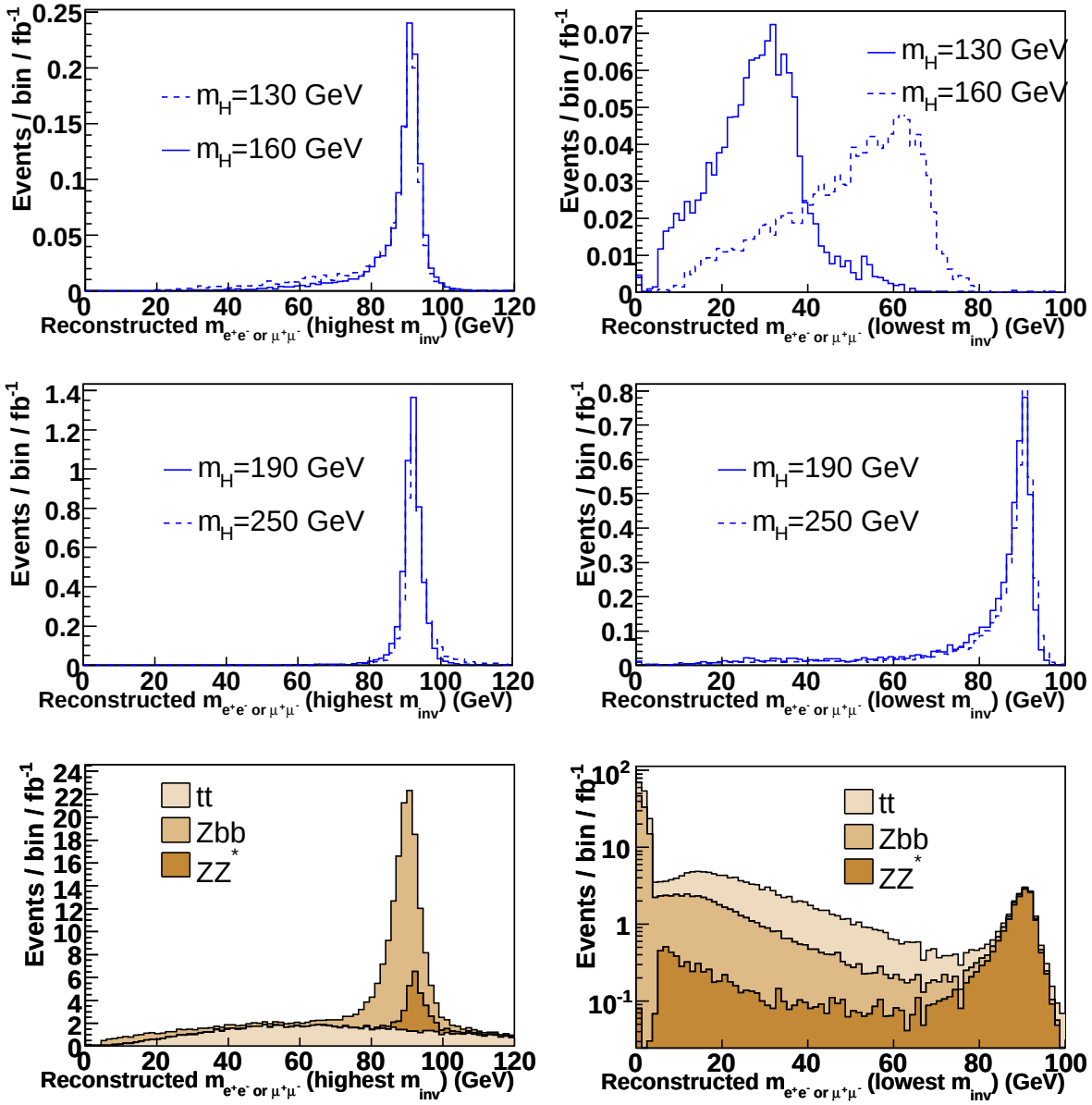

Figure 14: Invariant mass distributions for the reconstructed lepton pair (e^+e^- or $\mu^+\mu^-$) with the highest (left) and lowest (right) invariant mass, for m_H = 130, 160, 190 and 250 GeV, and for the three backgrounds.

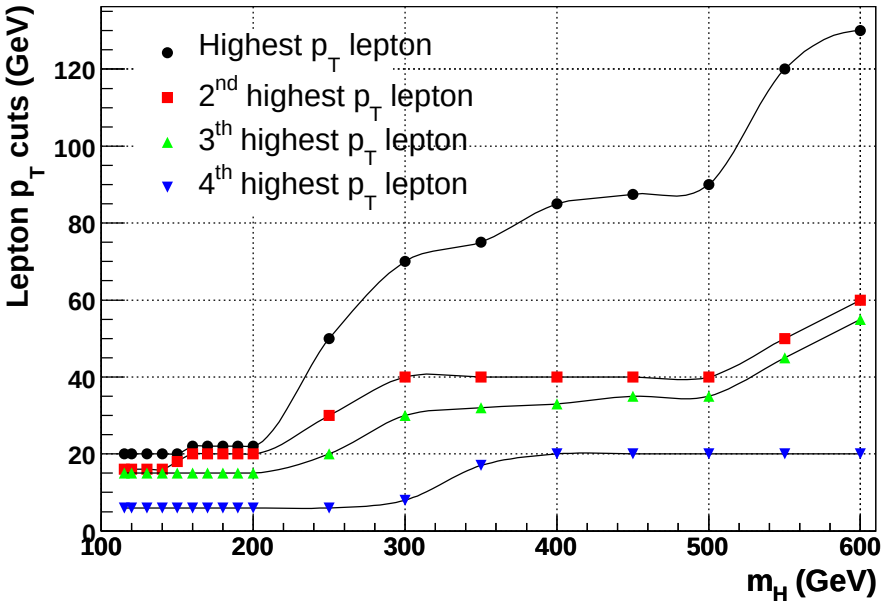

Figure 15: Optimized lepton p_T thresholds (thr1 to thr4) as a function of $\mathrm{m_H}$.

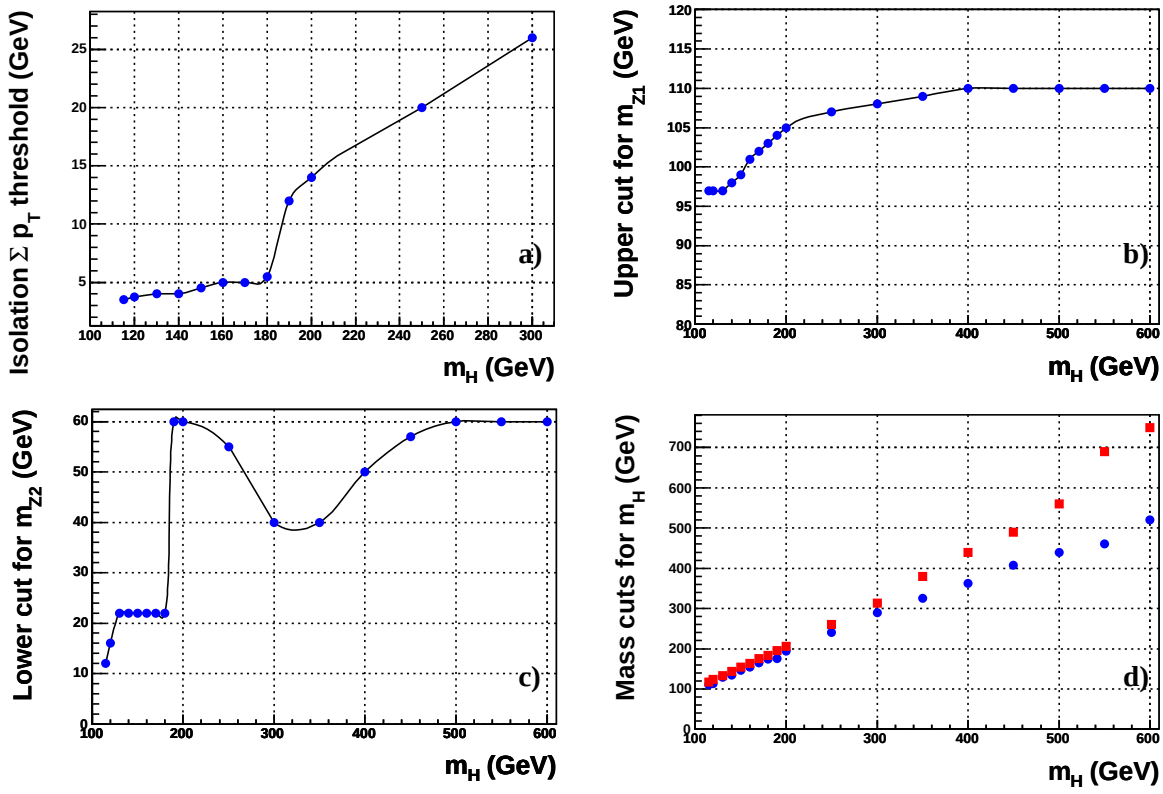

Figure 16: (a) Optimized isolation Σp_T threshold (no cut is applied for $\mathrm{m_H} > 300$ GeV). (b) Optimized upper threshold on the mass of the highest mass reconstructed Z (thr5). (c) Optimized lower thresholds on the mass of the lowest mass reconstructed Z (thr6). (d) Optimized upper and lower thresholds on the reconstructed $\mathrm{e^+e^-\mu^+\mu^-}$ invariant mass (thr8 and thr9).

7 Reconstructed Higgs Boson Mass Resolution

The invariant mass of the four reconstructed leptons, for events passing all cuts except for that around the Higgs boson mass, is shown in Figure 17 for three values of m_H.

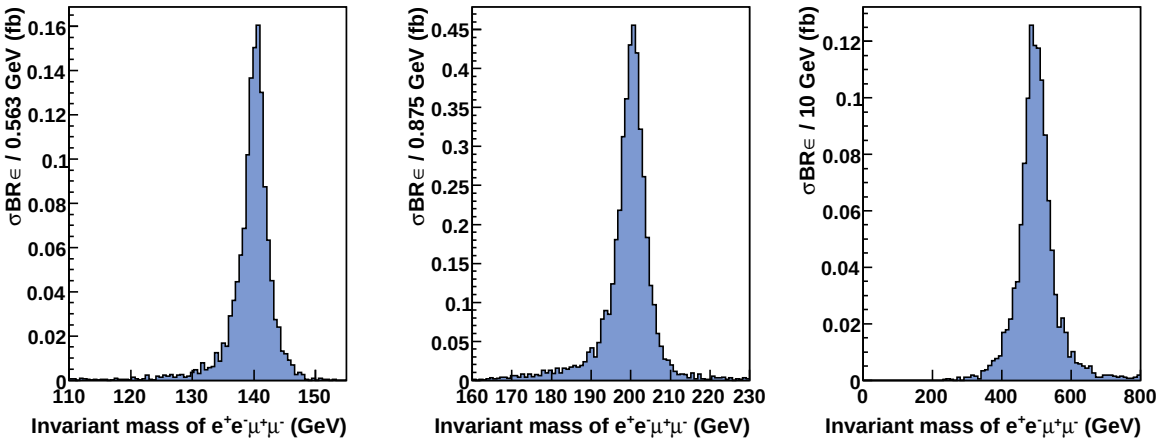

Figure 17: Invariant mass of the four reconstructed leptons, after all cuts except for that around the Higgs boson mass, for m_H = 140, 200 and 500 GeV.

The mass resolution achievable is estimated from the width of the distribution $\frac{m_H^{rec}}{m_H^{True}}$ and shown in Figure 18 as a function of m_H^{True}. It can be seen that the Higgs boson mass is reconstructed to within 1.2 and 1.35% of the generated value.

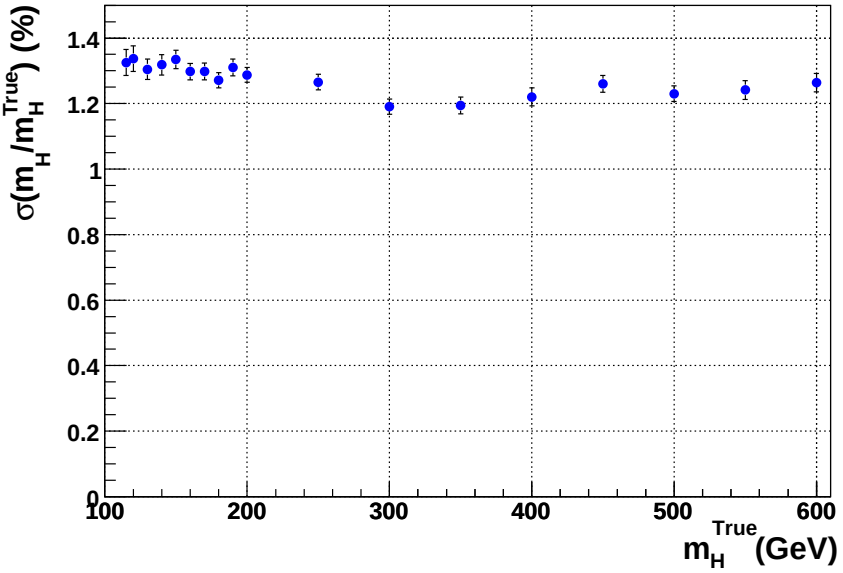

Figure 18: Expected experimental resolution on the Higgs boson mass as a function of the true mass value.

8 Results

Tables 5 and 6 summarize the expected cross-sections after each online and offline selection step, for Higgs boson masses of 140 GeV and 200 GeV, respectively. Values are shown for signal and for each of the three background processes.

Figure 19 shows the cross-section times branching ratio times efficiency after each stage of the online and offline event selection, for Higgs boson masses of 120 GeV, 150 GeV, 200 GeV and 400 GeV, and for each of the three backgrounds (at assigned Higgs boson mass).

Tables 7 and 8 show the branching ratio to four leptons, the preselection efficiency and the efficiency of each step in the online and offline selections, for Higgs boson masses of 140 GeV and 200 GeV, respectively, and for each of the three backgrounds.

The offline selection efficiency for the signal after all selections is shown as a function of $\mathrm{m_H}$ in Figure 20.

	Signal	$\mathrm{t\bar{t}}$	$\mathrm{Zb\bar{b}}$	$\mathrm{ZZ^\star/\gamma^\star}$
Production cross-section (NLO)	33.6×10^3	840×10^3	555×10^3	28.9×10^3
$\sigma\cdot$BR(4 lepton final state)	11.6	-	-	367.5
Preselection: $\sigma\times\mathrm{BR}\times\epsilon$	3.29±0.04	743±2	390±1	37.0±0.4
Level-1 trigger	3.24±0.04	707±2	360±1	36.3±0.4
High Level trigger	2.91±0.03	282±1	237±1	32.5±0.4
$\mathrm{e^+e^-\mu^+\mu^-}$reconstructed	2.23±0.03	130±1	141±1	24.1±0.3
Vertex and impact parameter cuts	2.01±0.03	18.9±0.3	18.4±0.2	21.5±0.3
Isolation cuts	1.83±0.03	1.34±0.07	5.8±0.1	20.0±0.3
Lepton p_T cuts	1.61±0.03	0.40±0.04	0.56±0.03	17.6±0.3
Z mass window cuts	1.35±0.02	0.20±0.03	0.23±0.02	13.8±0.3
Higgs boson mass window cuts	1.17±0.02	0.02±0.01	0.025±0.007	0.15±0.03
Expected events for $\int\mathcal{L}=10\ \mathrm{fb^{-1}}$	11.7±0.2	0.2±0.1	0.25±0.07	1.5±0.3

Table 5: Summary of cross-sections after each online and offline selection step, for $\mathrm{m_H}$=140 GeV, for signal and backgrounds. All values are expressed in fb, except for the expected number of events. Errors are statistical only.

Figure 21 shows the invariant mass of the four reconstructed leptons before and after the offline selection, for signal events with $\mathrm{m_H} = 140$ GeV (left) and $\mathrm{m_H} = 200$ GeV (right), and for the three background processes. It can be seen that for both low and high Higgs boson masses, the signal is clearly distinguishable above the background, which is dominated by the irreducible ZZ background.

Figure 22(a) shows the final cross-section times branching ratio times selection efficiency, for signal and background, as a function of the Higgs boson mass. The signal to background ratio is shown in Figure 22(b). The value of this ratio is between 1 and 7 for $\mathrm{m_H} > 120$ GeV, and between 1 and 3.5 for $\mathrm{m_H} \geq 170$ GeV. The number of expected events passing all selections for 10 $\mathrm{fb^{-1}}$ of integrated luminosity is shown in Table 9 for several values of the Higgs boson mass.

	Signal	$t\bar{t}$	$Zb\bar{b}$	$ZZ^{\star}/\gamma^{\star}$
Production cross-section (NLO)	17.9×10^3	840×10^3	555×10^3	28.9×10^3
$\sigma\cdot$BR(4 lepton final state)	23.8	-	-	367.5
Preselection: $\sigma\times$BR$\times\epsilon$	7.39±0.09	743±2	390±1	37.0±0.4
Level-1 trigger	7.36±0.09	707±2	360±1	36.3±0.4
High Level trigger	6.82±0.08	282±1	237±1	32.5±0.4
$e^+e^-\mu^+\mu^-$reconstructed	5.51±0.07	130±1	141±1	24.1±0.3
Vertex and impact parameter cuts	5.03±0.07	18.9±0.3	18.4±0.2	21.5±0.3
Isolation cuts	4.92±0.07	5.1±0.1	12.3±0.2	21.3±0.3
Lepton p_T cuts	4.78±0.07	1.93±0.09	1.78±0.06	18.7±0.3
Z mass window cuts	4.45±0.07	0.15±0.03	0.12±0.02	14.4±0.3
Higgs boson mass window cuts	3.64±0.06	0.006±0.005	0.006±0.003	1.61±0.09
Expected events for $\int\mathcal{L}=10$ fb^{-1}	36.4±0.6	0.06±0.05	0.06±0.03	16.1±0.9

Table 6: Summary of cross-section after each online and offline selection step, for m_H=200 GeV, for signal and backgrounds. All values are expressed in fb, except for the expected number of events. Errors are statistical only.

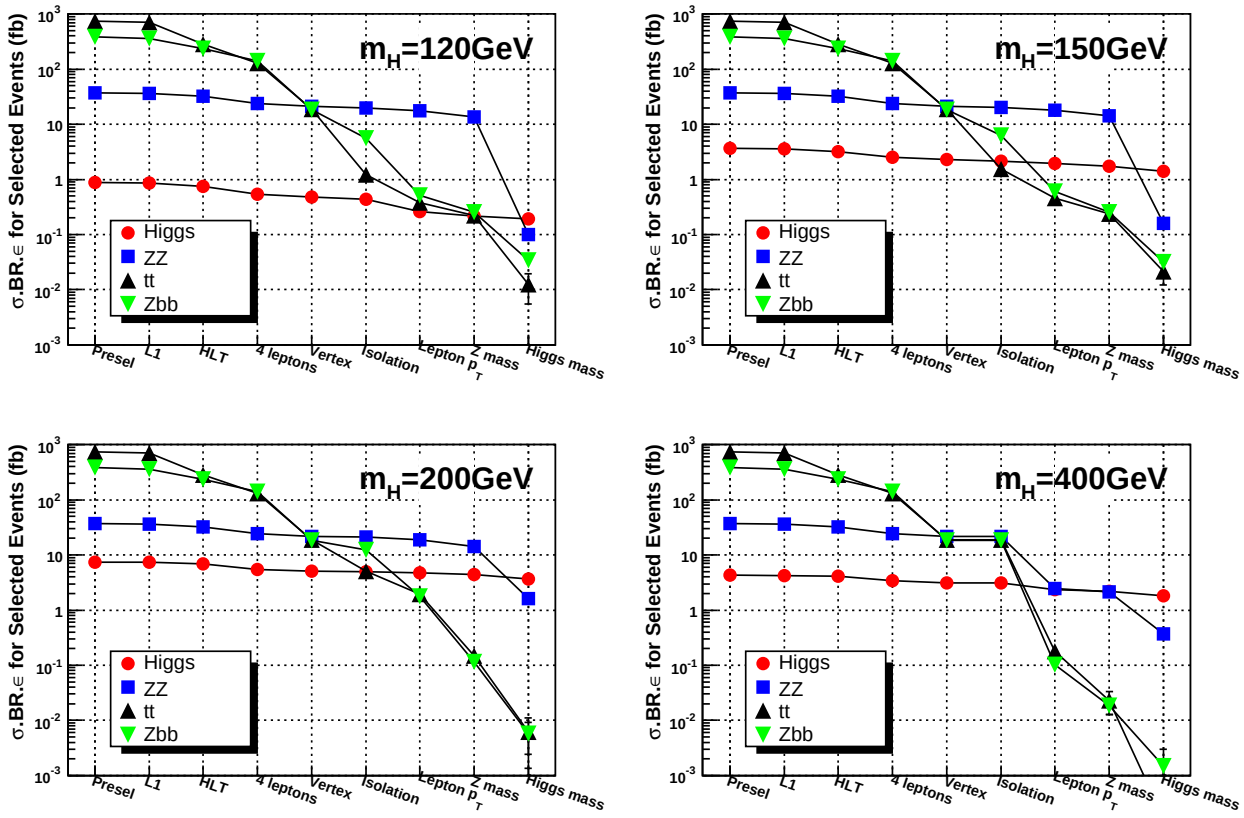

Figure 19: Production cross-section times branching ratio times efficiency after each stage of the online and offline event selection, for Higgs boson masses of 120 GeV, 150 GeV, 200 GeV and 400 GeV, and for each of the three backgrounds (at assigned Higgs mass).

	Signal	$t\bar{t}$	$Zb\bar{b}$	$ZZ^\star/\gamma^\star$
BR(4 lepton final state)	0.035	-	-	1.27
Preselection	27.2	-	-	9.41
Level-1 trigger	98.5±0.1	95.1±0.1	92.3±0.1	97.9±0.2
High Level trigger	90±0.3	39.9±0.1	65.8±0.1	89.6±0.4
$e^+e^-\mu^+\mu^-$reconstructed	76.6±0.5	46.1±0.2	59.5±0.1	74.2±0.6
Vertex and impact parameter cuts	90.1±0.4	14.5±0.2	13±0.1	89±0.5
Isolation cuts	91.2±0.4	7.11±0.40	31.6±0.5	92.9±0.4
Lepton p_T cuts	87.8±0.5	29.8±2.7	9.57±0.57	88.2±0.5
Z mass window cuts	84.2±0.6	49.3±5.4	40.9±3.1	78.1±0.7
Higgs boson mass window cuts	86.5±0.6	11.6±4.9	10.9±3.0	1.11±0.2
Final efficiency w.r.t. HLT	40.2±0.6	0.0081±0.0036	0.010±0.003	0.469±0.086

Table 7: Branching ratio to four leptons, preselection efficiency and efficiency of each step in the online and offline selections, for a Higgs boson mass of 140 GeV, and for backgrounds. All values are expressed in %.

	Signal	$t\bar{t}$	$Zb\bar{b}$	$ZZ^\star/\gamma^\star$
BR(4 lepton final state)	0.13	-	-	1.27
Preselection	29.6	-	-	9.41
Level-1 trigger	99.5±0.1	95.1±0.1	92.3±0.1	97.9±0.2
High Level trigger	92.7±0.3	39.9±0.1	65.8±0.1	89.6±0.4
$e^+e^-\mu^+\mu^-$reconstructed	80.9±0.5	46.1±0.2	59.5±0.1	74.2±0.6
Vertex and impact parameter cuts	91.3±0.4	14.5±0.2	13.0±0.1	89.0±0.5
Isolation cuts	97.8±0.2	26.8±0.7	66.9±0.5	99.2±0.1
Lepton p_T cuts	97.2±0.2	38.2±1.5	14.5±0.5	88.0±0.5
Z mass window cuts	93.1±0.4	7.65±1.30	6.47±0.86	76.6±0.7
Higgs boson mass window cuts	81.8±0.6	4.19±3.53	5.03±2.99	11.2±0.6
Final efficiency w.r.t. HLT	53.4±0.6	0.0022±0.0019	0.0025±0.0015	4.95±0.27

Table 8: Branching ratio to four leptons, preselection efficiency and efficiency of each step in the online and offline selections, for a Higgs boson mass of 200 GeV, and for backgrounds. All values are expressed in %.

m_H (GeV)	120	130	140	150	160	170	180	200	250	300	400	500
N signal for 10 fb^{-1}	1.9	4.6	11.7	14.1	7.8	3.8	8.7	36.4	29.1	19.4	18.0	9.6
N back for 10 fb^{-1}	1.5	0.6	2.0	2.1	2.0	2.9	4.0	16.2	13.6	4.1	3.7	2.6

Table 9: Expected number of events from signal and background processes after all selections for an integrated luminosity of 10 fb^{-1}.

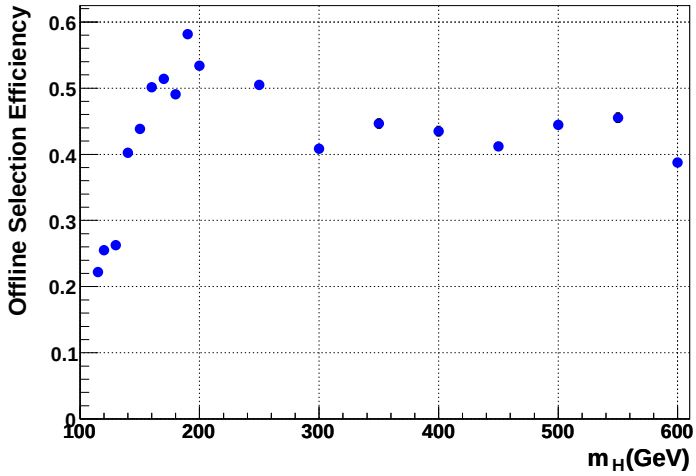

Figure 20: Offline selection efficiency after all selections for the signal, as a function of m_H.

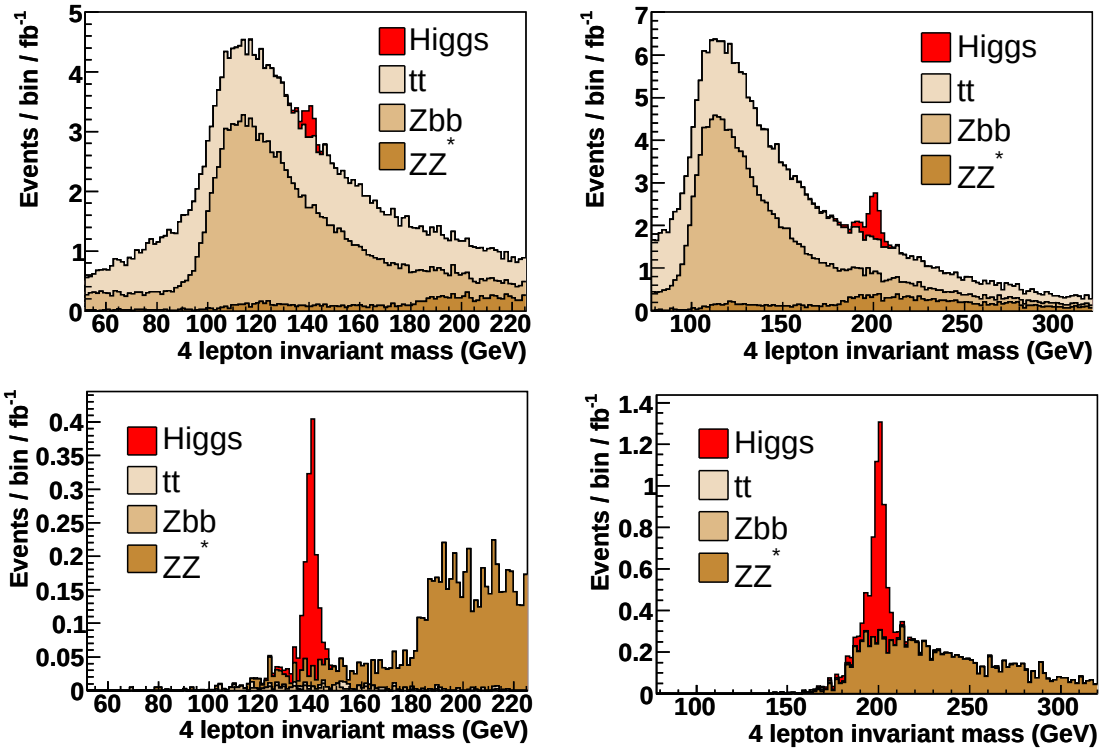

Figure 21: Invariant mass of the four reconstructed leptons before (top) and after (bottom) offline selection, for signal events with $m_H = 140$ GeV (left) and $m_H = 200$ GeV (right), and for the three background processes.

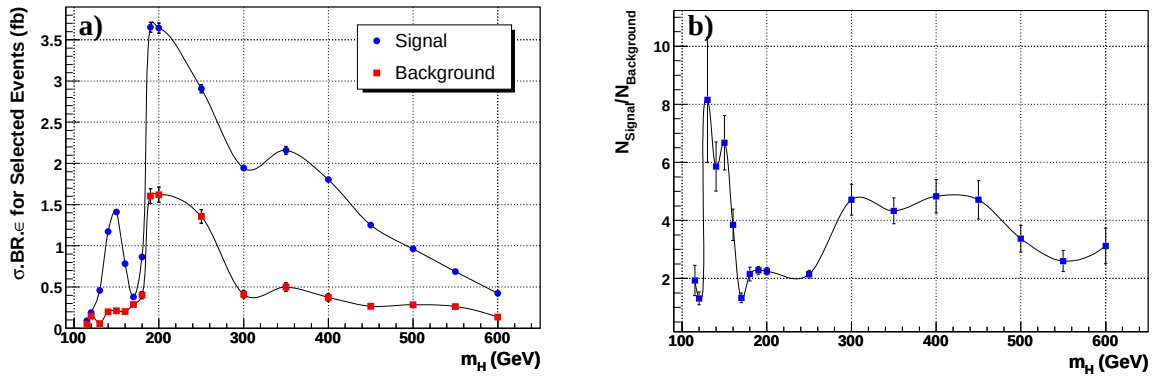

Figure 22: (a) Cross-section times branching ratio times efficiency after all selections, and (b) signal to background ratio after all selections, as a function of the Higgs boson mass.

8.1 Statistical Significance

The statistical significance of an excess of observed events, N_{obs}, with respect to the number of events expected from background processes, $\mu_{\rm B}$, is calculated using the estimator S_{cP}. The number of sigmas of a Gaussian distribution equivalent to the Poisson probability of observing equal to or greater than N_{obs} events, given $\mu_{\rm B}$ expected events, is calculated:

$$\frac{1}{\sqrt{2\pi}}\int_{S_{cP}}^{\infty} e^{-\frac{x^2}{2}}dx = \sum_{i=N_{obs}}^{\infty}\frac{(\mu_B)^i e^{-\mu_B}}{i!} \qquad (2)$$

The S_{cP} estimator can be used to calculate the significance taking into account experimental and theoretical systematic uncertainties.

Figure 23 shows the S_{cP} significance after all selection cuts for integrated luminosities of 10 fb^{-1} and 30 fb^{-1}, with and without taking into account the systematic error on the background estimation. The systematic error on the background will be discussed in Section 9. Figure 24 shows the integrated luminosity required to obtain a significance of 5σ using the H $\rightarrow$ ZZ$^{(\star)}$ $\rightarrow$ 2e2μ channel, with and without the systematic error on the background. It can be seen that a significance of 5σ can be achieved with less than 30 fb^{-1} of integrated luminosity for a Higgs boson with mass in the range $130 \leq {\rm m_H} \leq 500$ GeV, excluding a gap of about 15 GeV close to $\rm m_H$ = 170 GeV, for which close to 100 fb^{-1} are required. If the Higgs boson mass lies in the range $190 \leq {\rm m_H} \leq 400$ GeV, 5σ significance can be attained with less than 8 fb^{-1} of integrated luminosity.

The high significance at $\rm m_H$=150 GeV is due to a combination of high signal cross-section times branching ratio and low background. The low significance at $\rm m_H$=170 GeV is due to the suppression of the $H \rightarrow ZZ^{(\star)}$ branching ratio at the $H \rightarrow WW$ turn on. Although the background is large at $\rm m_H$=200 GeV, the significance is high due to the strong enhancement of the $H \rightarrow ZZ^{(\star)}$ branching ratio for ${\rm m_H} > 2{\rm m_Z}$. The drop in significance at $\rm m_H$=250 GeV results from the reduced signal cross-section whilst the ZZ$^\star/\gamma^\star$ background remains high. The secondary peak at $\rm m_H$=350 GeV corresponds to the maximum of the $H \rightarrow ZZ^{(\star)}$ branching ratio beyond which $H \rightarrow t\bar{t}$ is kinematically allowed and corresponds to the shoulder seen at this value in Figure 4. The shoulder seen at $\rm m_H$=550 GeV is due to a reduced signal to

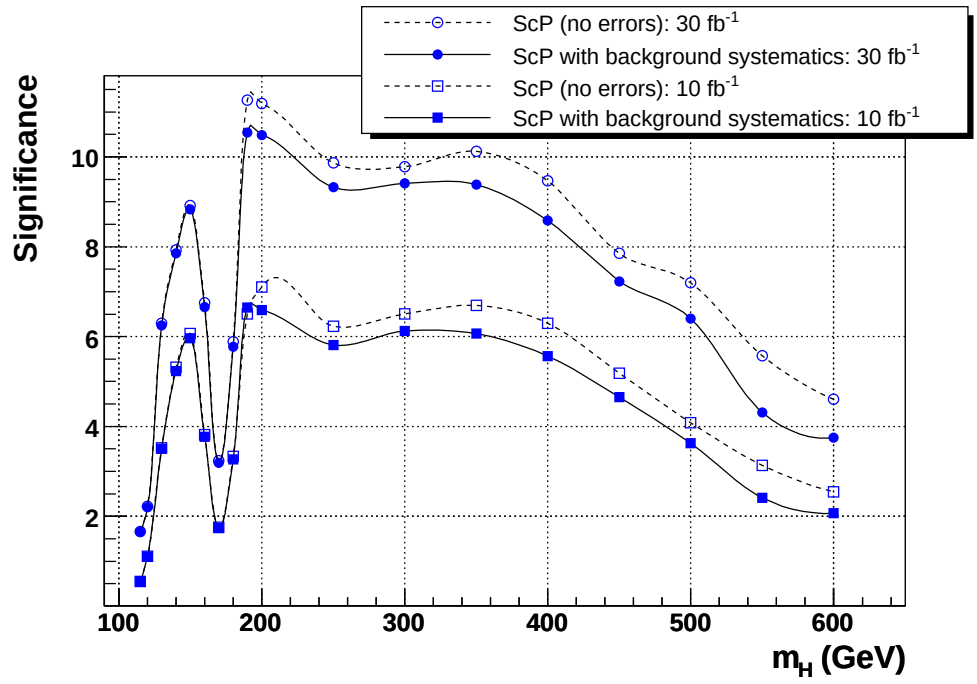

Figure 23: Significance, as defined in Equation 2 after all selection cuts for integrated luminosities of 10 fb^{-1} and 30 fb^{-1}, with and without taking into account the systematic error on the background estimation.

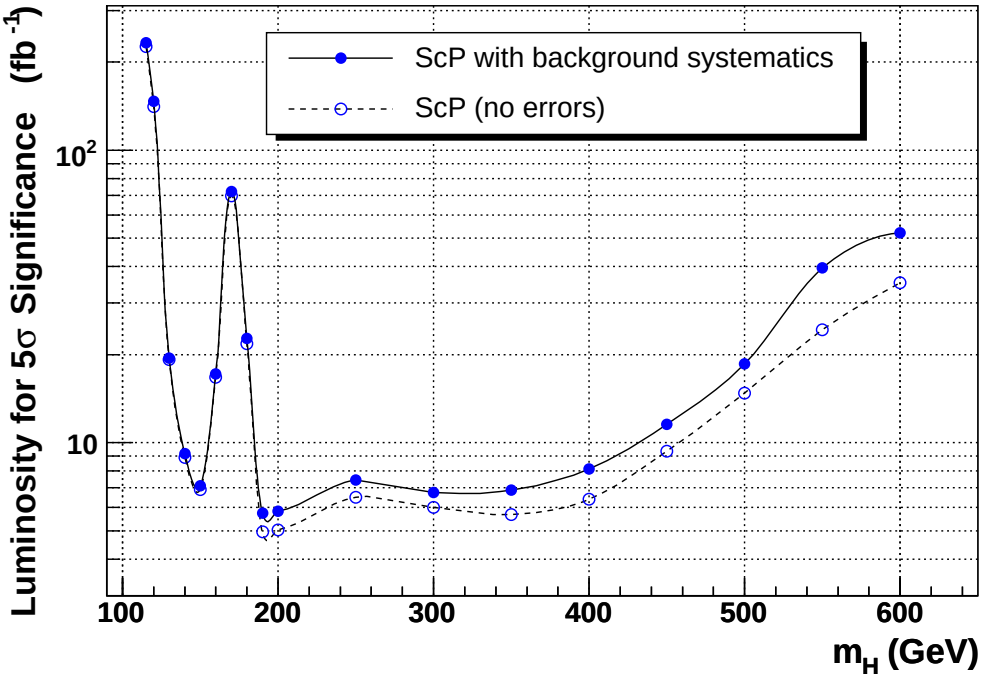

Figure 24: Integrated luminosity required to obtain a significance of 5σ using the $H \rightarrow ZZ^{(\star)} \rightarrow 2e2\mu$ channel, with and without the systematic error on the background estimation taken into account.

background ratio at this mass due to the large width of the signal peak in a region where the $ZZ^{\star}/\gamma^{\star}$ background is still significant.

Table 10 shows the expected number of events from signal and background processes after all selections, for an integrated luminosity corresponding to 5σ significance.

m_H (GeV)	120	130	140	150	160	170
N signal at $\int \mathcal{L}$ for 5σ	28.0±0.7	8.9±0.2	10.7±0.2	10.0±0.2	13.4±0.2	27.5±0.5
N back at $\int \mathcal{L}$ for 5σ	21.4±3.6	1.1±0.3	1.8±0.3	1.5±0.2	3.5±0.5	20.7±2.6
m_H (GeV)	180	200	250	300	400	500
N signal at $\int \mathcal{L}$ for 5σ	19.6±0.3	21.2±0.4	21.7±0.4	13.1±0.3	14.6±0.3	17.8±0.3
N back at $\int \mathcal{L}$ for 5σ	9.1±1.0	9.4±0.5	10.1±0.6	2.8±0.3	3.0±0.4	5.3±0.7

Table 10: Expected number of events from signal and background processes after all selections for an integrated luminosity corresponding to 5σ significance, using the $H \rightarrow ZZ^{(\star)} \rightarrow 2e2\mu$ channel.

9 Evaluation of Background from Data

Since the production cross-section for the irreducible $ZZ^{\star}/\gamma^{\star}$ background is not known with high accuracy, it is proposed to measure the size of the background directly from the data, using the sidebands in the reconstructed four-lepton invariant mass distribution. Figure 25 shows the number of expected events from simulated signal and background for an integrated luminosity corresponding to a 5σ discovery significance, for Higgs boson masses of 140 and 200 GeV. The integrated luminosities corresponding to 5σ discovery significance for m_H =140 GeV and m_H =200 GeV are 9.2 and 5.8fb^{-1}, respectively (Figure 24). Superimposed on Figure 25 is a toy Monte Carlo simulation of what the LHC data might look like: The total number of events in the toy Monte Carlo is generated randomly from a Poisson distribution with mean equal to the total number of expected events from all processes (signal plus background). For each event, the four lepton invariant mass is generated randomly according to the histogram formed from the sum of the expected distributions for signal and all backgrounds.

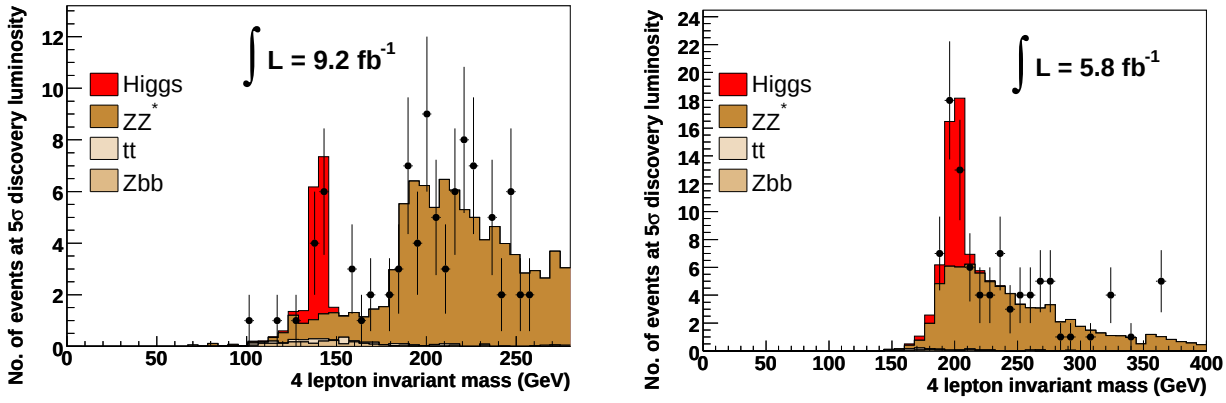

Figure 25: Number of expected events for signal and background for an integrated luminosity corresponding to a discovery significance of 5σ, for Higgs boson masses of 140 and 200 GeV. A toy Monte Carlo based on the histograms is superimposed to simulate LHC data.

Measurement of the background from sidebands requires that the position of the signal peak is well defined, and it is clear in Figure 25 that this is the case at luminosities corresponding to the

discovery significance. It can also be seen that the number of events outside the Higgs boson mass window cuts (signal region) which will be used to measure the size of the background is of order several tens of events.

The number of background events measured from the data within the signal region, N_{Data}^{IN}, is calculated as:

$$N_{Data}^{IN} = \alpha_{MC} N_{Data}^{OUT}, \qquad \text{where} \qquad \alpha_{MC} = \frac{N_{MC}^{IN}}{N_{MC}^{OUT}} \tag{3}$$

N_{Data}^{OUT} is the number of observed events lying outside the signal region and α_{MC} is the ratio of the number of background events inside the signal region (N_{MC}^{IN}) to outside the signal region (N_{MC}^{OUT}), as determined from the background simulated events.

The error on the number of background events in the signal region measured using this method is given by $\Delta B = \Delta B_{stat} \oplus \Delta B_{Theory}$, where $\Delta B_{stat} = \alpha_{MC}\sqrt{N_{Data}^{OUT}}$ is the dominant contribution to the total uncertainty. The relative statistical error on the background, $\frac{\Delta B_{stat}}{B_{stat}}$, can be written as $(N_{Data}^{OUT})^{-\frac{1}{2}}$ and it is shown as a function of $\mathrm{m_H}$ in Figure 26, for an integrated luminosity corresponding to 5σ significance. The value is generally small for $\mathrm{m_H} < 2\mathrm{m_Z}$ due to the large amount of data in the side bands relative to within the signal region[1)], as seen in the left hand plot in Figure 25. The structure seen at low $\mathrm{m_H}$ is due to the variation in the luminosity corresponding to 5σ significance as a function of $\mathrm{m_H}$ seen in Figure 24. For large $\mathrm{m_H}$, the sidebands are suppressed by the hard cuts on the lepton p_T (Figure 15) [2)]. The fluctuations for $\mathrm{m_H} > 400$ GeV are a result of limited Monte Carlo statistics in the sidebands.

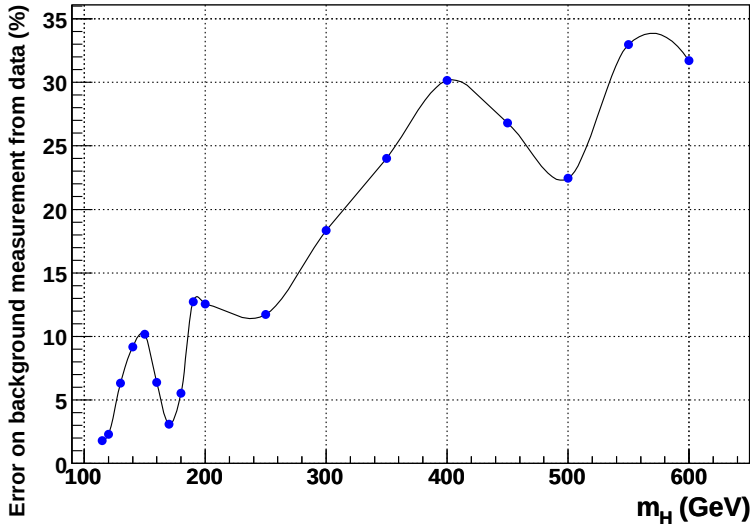

Figure 26: Error on measurement from data of the number of background events within the signal region, as a percentage of the expected number of background events within the signal region.

[1)] The sidebands are not suppressed due to the lack of any upper cut applied to the off-shell Z boson (see Section 6.3).

[2)] It should be possible to increase the amount of data in the sidebands at high $\mathrm{m_H}$ with little impact on the significance by loosening the lepton p_T cuts.

ΔB_{Theory} is the theoretical uncertainty on the shape of the $m_{4\ell}$ distribution for the $ZZ^{\star}/\gamma^{\star}$ background. The value is taken from [11], which takes into account PDF and QCD scale uncertainties in the $ZZ^{\star}/\gamma^{\star}$ production cross-section at NLO, and varies between 0.5% and 4.5% for the range of Higgs boson masses considered, with the minimum value at $\mathrm{m_H}$=250 GeV.

10 Measurement of the properties of the Higgs Boson

The $H \rightarrow ZZ^{(\star)} \rightarrow 4\ell$ channel can be used to evaluate the mass, width and production cross-section of the Higgs boson.

10.1 Mass Measurement

The mass of the Higgs boson can be evaluated by fitting a Gaussian to the mass peak discussed in Section 7. In the high statistics limit represented by the simulated signal, the ratio of the mass obtained from a Gaussian fit to the reconstructed $m_{4\ell}$ distribution, to the true mass, is found to be 1 to within $\pm$0.3% for all $\mathrm{m_H}$ (Figure 27).

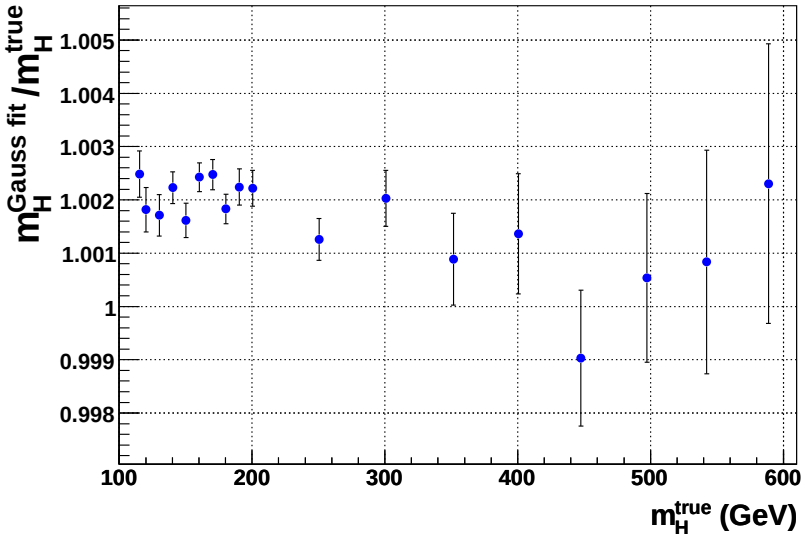

Figure 27: Ratio of the mass obtained from a Gaussian fit to the reconstructed $m_{4\ell}$ distribution, to the true mass, as a function of $\mathrm{m_H}$, in high statistics limit represented by the simulated signal.

Figure 28 shows the statistical error on the Higgs boson mass measurement, given by $\Delta m_H^{stat} = \sigma_{Gauss}/\sqrt{N_S}$, where σ_{Gauss} is the width of the gaussian fit to the peak from the simulated signal and N_S is the expected number of signal events passing all selections, for integrated luminosities of 10 and 30 fb^{-1}, and for the integrated luminosity corresponding to 5σ significance, as a function of the true Higgs boson mass.

10.2 Width Measurement

Figure 29 shows the measured width of the Higgs boson mass peak, obtained from a Gaussian fit to the reconstructed $\mathrm{e^+e^-\mu^+\mu^-}$ invariant mass peak from the simulated signal, as a

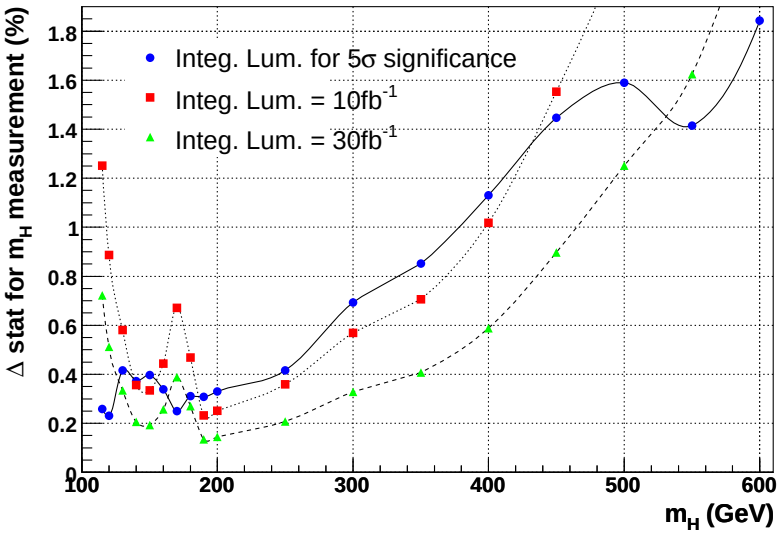

Figure 28: Statistical error on the Higgs boson mass measurement for integrated luminosities of 10 and 30 fb^{-1}, and for the integrated luminosity corresponding to 5σ significance, as a function of $\mathrm{m_H}$.

function of $\mathrm{m_H}$. The true width from theory Γ_H is also shown. The measured width is the sum in quadrature of the natural width and the contribution to the width from the experimental measurement, arising from inaccuracies in the reconstruction of the lepton momenta. It can be seen that for $\mathrm{m_H}$ less than around 200 GeV, the measured width is completely dominated by the experimental width. The statistical uncertainty on the width measurement, given by $(\Delta\Gamma^{rec})_{stat} = \sigma_{Gauss}/\sqrt{2N_S}$, where σ_{Gauss} is the width of Gaussian fit to the peak and N_S is the expected number of signal events passing all selections; Figure 30 shows the relative statistical uncertainty, $\frac{(\Delta\Gamma^{rec})_{stat}}{\Gamma^{true}}$, as a function of $\mathrm{m_H}$. The uncertainty is shown separately for integrated luminosities of 10 and 30 fb^{-1}, and for the integrated luminosity corresponding to 5σ significance, as a function of $\mathrm{m_H}$. The direct measurement of the Higgs boson width is possible with $\frac{(\Delta\Gamma^{rec})_{stat}}{\Gamma^{true}} < 30\%$ for $\mathrm{m_H}$ $\geq$200 GeV.

10.3 Production Cross-Section Measurement

The Higgs boson production cross-section can be determined from the number of observed events N_{obs} after all selections, given the efficiency ϵ of the event selection and the integrated luminosity $\mathcal{L}$: $\sigma = N_{obs}/\mathcal{L}\epsilon$.

The total uncertainty on the cross-section measurement is given by:

$$\Delta\sigma^2 = \Delta\sigma^2_{stat} + \Delta\sigma^2_{syst} + \Delta\mathcal{L}^2 + \Delta B^2$$

where $\Delta\sigma_{stat}$, $\Delta\sigma_{syst}$, $\Delta\mathcal{L}$ and ΔB are the statistical error, the systematic uncertainty from the event selection, the uncertainty on the luminosity measurement and the background systematic uncertainty, respectively.

The statistical uncertainty $\Delta\sigma_{stat} = \sqrt{N_{exp}}$, where N_{exp} is the expected number of events (signal plus background) passing all selections, is shown as a fraction of the expected number of signal events, in Figure 31 for integrated luminosities of 10 and 30 fb^{-1}, and for the integrated luminosity corresponding to 5σ significance, as a function of $\mathrm{m_H}$.

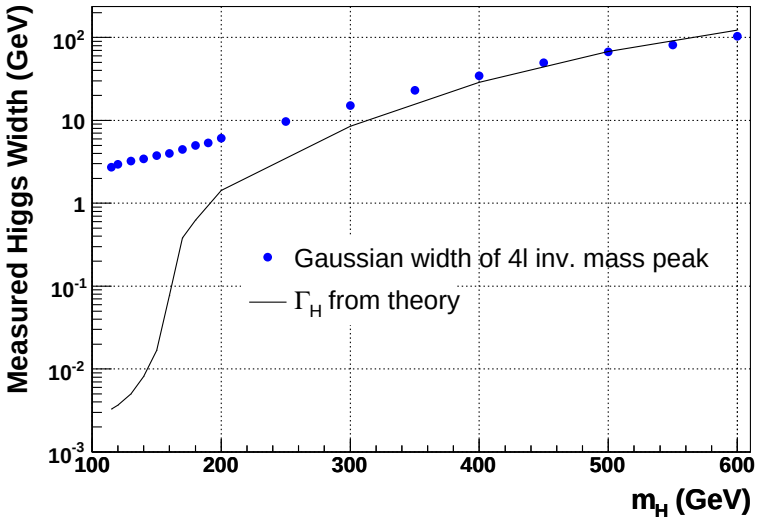

Figure 29: Measured width of the Higgs boson mass peak, obtained from a Gaussian fit to the peak, as a function of the true Higgs boson mass. The true width from theory is also shown.

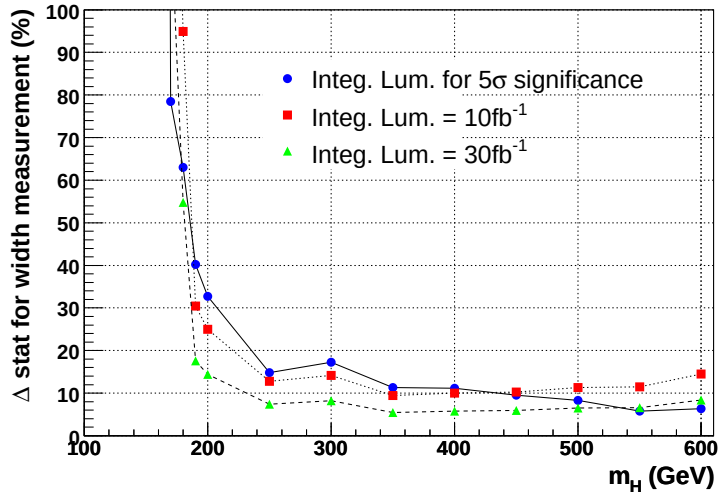

Figure 30: Statistical error on the Higgs boson width measurement for integrated luminosities of 10 and 30 fb^{-1}, and for the integrated luminosity corresponding to 5σ significance, as a function of $\mathrm{m_H}$.

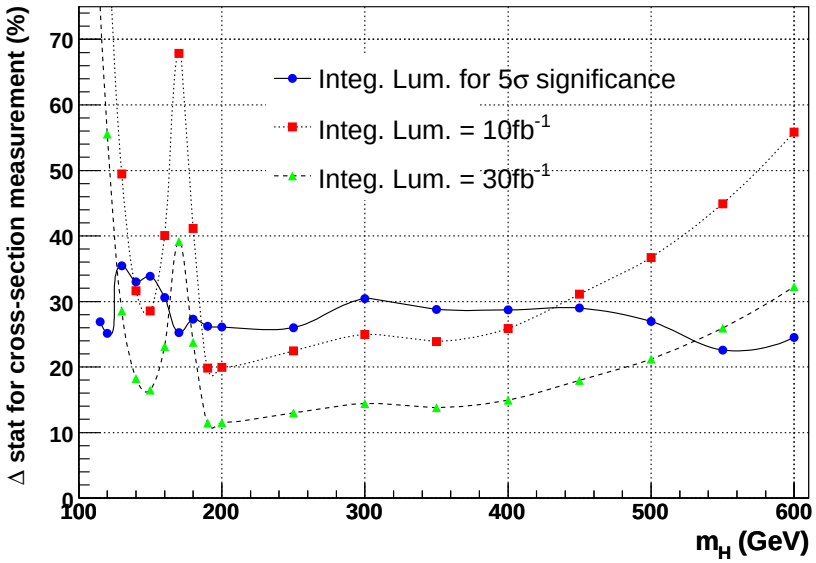

Figure 31: Statistical uncertainty on the Higgs boson production cross-section for integrated luminosities of 10 and 30 fb^{-1}, and for the integrated luminosity corresponding to 5σ significance, as a function of $\mathrm{m_H}$.

The total systematic error arising from the offline reconstruction and event selection can be summarized as:

$$\Delta\sigma^2_{syst} = 2\Delta\epsilon^2_{\mathrm{e}} + 2\Delta\epsilon^2_{\mu} + \Delta\epsilon^2_{iso}$$

where $\Delta\epsilon_{\mathrm{e}}$ is the uncertainty in the reconstruction efficiency for electrons, estimated to be around 1% per electron [17], $\Delta\epsilon_{\mu}$ is the uncertainty in the muon reconstruction efficiency, which has been shown to be measurable to be better than 1% per muon [11], and $\Delta\epsilon_{iso}$ is the uncertainty in the efficiency of the isolation cut, estimated in the $\mathrm{H} \rightarrow \mathrm{ZZ}^{(\star)} \rightarrow 4\mu$ analysis [11] to be around 2% per event. This gives a total $\Delta\sigma_{syst}$ =3%.

The uncertainty on the measurement of the LHC luminosity $\Delta\mathcal{L}$ is expected to be around 3%. The uncertainty on the background, ΔB, was discussed in Section 9 and was shown as a function of $\mathrm{m_H}$ in Figure 25.

11 Summary

The Standard Model Higgs boson with mass in the range $130 \leq \mathrm{m_H} \leq 500$ GeV is observable at CMS with greater than 5σ significance through the channel $\mathrm{H} \rightarrow \mathrm{ZZ}^{(\star)} \rightarrow 2\mathrm{e}2\mu$ alone with less than 30 fb^{-1} of integrated luminosity. For a small mass range close to $\mathrm{m_H}$ = 170 GeV, where the branching ratio to ZZ* is suppressed, about 100 fb^{-1} are required. If the Higgs boson mass lies in the range $190 \leq \mathrm{m_H} \leq 400$ GeV, 5σ significance can be attained through this channel with less than 9 fb^{-1} of integrated luminosity. When the $\mathrm{H} \rightarrow \mathrm{ZZ}^{(\star)} \rightarrow 2\mathrm{e}2\mu$ channel will be combined with the $\mathrm{H} \rightarrow \mathrm{ZZ}^{(\star)} \rightarrow 4\mathrm{e}$ and $\mathrm{H} \rightarrow \mathrm{ZZ}^{(\star)} \rightarrow 4\mu$ channels, the integrated luminosity required for discovery will be significantly reduced. For $\mathrm{m_H} < 130$ GeV and $160 \leq \mathrm{m_H} \leq 180$ GeV, the $\mathrm{H} \rightarrow \mathrm{ZZ}^{(\star)} \rightarrow 4\ell$ result will be combined with the $\mathrm{H} \rightarrow \gamma\gamma$ and $\mathrm{H} \rightarrow \mathrm{W}^+\mathrm{W}^- \rightarrow 2\ell 2\nu$ channels, respectively, which are more sensitive channels in these mass ranges.

The signal to background ratio for the $H \rightarrow ZZ^{(\star)} \rightarrow 2e2\mu$ channel is between 1 and 7 for $m_H > 120$ GeV, and between 1 and 3.5 for $m_H \geq 170$ GeV.

Direct measurement of the mass of the Higgs boson can be performed with the integrated luminosity corresponding to 5σ significance with statistical error smaller than 0.4% for $m_H < 300$ GeV, and smaller than 1.2% for all m_H values. Direct measurement of the Higgs boson width is possible for $m_H >$200 GeV.

A Correction for Effect of Forcing Leptonic Tau Decay

The forcing of taus to decay to electrons or muons has the consequence that events in which one or both Zs decay to taus are over-represented in the generated event samples because their suppression due to the $\tau \to e/\mu$ branching ratio is absent. To account for this in the determination of selection efficiencies, events are counted separately in each of the three cases:

1. $Z_1 \to \ell\ell$, $Z_2 \to \ell\ell$ ($\ell =$ e or μ)
2. $Z_1 \to \ell\ell$, $Z_2 \to \tau\tau$
3. $Z_1 \to \tau\tau$, $Z_2 \to \tau\tau$

The production cross-section times branching ratio to four leptons times preselection efficiency is given by:

$$\sigma \cdot \mathrm{BR} \cdot \epsilon = \sigma(\mathrm{pp} \to \ \mathrm{H}) \cdot \mathrm{BR}(\mathrm{H} \to \ \mathrm{ZZ}) \cdot [\mathrm{BR}_1 \cdot \epsilon_1 + \mathrm{BR}_2 \cdot \epsilon_2 + \mathrm{BR}_3 \cdot \epsilon_3]$$

where BR_i is the branching ratio for each case, including BR($\tau \to$ e/μ), and

$$\epsilon_i = \frac{N^i_{preselected}}{N^i_{generated}} = \frac{N^i_{preselected}}{w_i \cdot N^{total}_{generated}}$$

where w_i is the fraction of generated events corresponding to each case:

- $w_1 = (2/3)^2 = 4/9$
- $w_2 = 2(2/3)(1/3) = 4/9$
- $w_3 = (1/3)^2 = 1/9$

These weights are propagated through all stages of the analysis. The above applies to signal samples and the $\mathrm{ZZ}^\star/\gamma^\star$ background. The $\mathrm{t\bar{t}}$ background, for which taus from the decay of the Ws are forced to decay leptonically, is treated similarly. No forcing of Z to leptons or tau to leptons was applied in the $\mathrm{Zb\bar{b}}$ background samples.

References

[1] The LEP Electroweak Working Group: http://lepewwg.web.cern.ch/LEPEWWG/

[2] ALEPH, DELPHI, L3 and OPAL Collaborations, "Search for the Standard Model Higgs Boson at LEP" Phys.Lett. **B565** (2003) 61-75, arXiv:hep-ex/0112021

[3] A. Djouadi, J. Kalinowski and M. Spira, "HDECAY: a program for Higgs Boson Decays in the Standard Model and its Supersymmetric Extension", arXiv:hep-ph/9704448.

[4] T. Sjostrand, L. Lonnblad and S. Mrenna, PYTHIA 6.2 Physics and Manual, report LU-TP-01-21, Aug 2001, arXiv:hep-ph/0108264.

[5] A. Pukhov, E. Boos, M. Dubinin et al, Aug 1999, arXiv:hep-ph/9908288

[6] E. Barberio and Z. Was, "PHOTOS - A universal Monte Carlo for QED radiative corrections: version 2.0", Comput. Phys. Commun. 79 (1994) 291-308.

[7] CMS Simulation Package CMSIM – User's Guide and Reference Manual, http://cmsdoc.cern.ch/cmsim/cmsim.html

[8] CMS OO Reconstruction – User's Guide and Reference Manual, http://cmsdoc.cern.ch/orca/

[9] M. Spira, "HIGLU: A Program for the Calculation of the Total Higgs Production Cross Section at Hadron Colliders via Gluon Fusion including QCD Corrections, arXiv:hep-ph/9510347;
M. Spira, Fortsch. Phys. 46 (1998) 203.

[10] F. Maltoni, "Theoretical Issues and Aims at the Tevatron and LHC", Talk on HCP2005, http://hcp-2005.web.cern.ch/HCP-2005.

[11] S. Abdullin et. al., "Search Strategy for the Standard Model Higgs Boson in the H$\rightarrow$ ZZ$\rightarrow 4\mu$ using $M(4\mu)$-Dependent Cuts" CMS NOTE-2006/122

[12] D. Acosta et. al., "NLO vs. LO: kinematical differences for signal and background in the H$\rightarrow$ ZZ$^{(\star)} \rightarrow 4\mu$ analysis" CMS NOTE-2006/130

[13] S. Baffioni et. al., "Electron reconstruction in CMS", CMS NOTE-2006/040

[14] T. Speer et al., "Vertex Fitting in the CMS Tracker", CMS NOTE-2006/032

[15] "MINUIT, Function Minimization and Error Analysis", CERN Program Library Long Writeup D506

[16] CMS Physics TDR, Volume 1, CERN-LHCC-2006-001, 2 February 2006

[17] S. Baffioni et. al. "Discovery potential for the SM Higgs boson in the H$\rightarrow$ ZZ$^{(\star)} \rightarrow$ $\mathrm{e^+e^-e^+e^-}$ decay channel" CMS NOTE-2006/115